Theranostics of Folic Acid Conjugated Cu on Te Nanocomposite: Fluorescence Sensing, Imaging and Selective Cytotoxicity towards HeLa Cells

Debashree Das[a,b*], Sampurna Bhattacharya[c], Shalmali Basu[a], Saptydeep Das[d], Ujjal Das[d], David J. Morgan[e], Kamalika Sen[a*]

[a]Department of Chemistry, University of Calcutta, 92 APC Road, Kolkata 700009, India
[b]Department of Chemistry, Bharat Institute of Engineering & Technology, Mangalpally, Ibrahimpatnam, Telangana 501510, India
[c]Department of Biophysics, Molecular Biology & Bioinformatics, University of Calcutta, 92 APC Road, Kolkata 700009, India
[d]UGC-DAE Consortium for Scientific Research, Kolkata Centre, III/LB-8, Bidhannagar, Kolkata, 700098, India
[e]Cardiff Catalysis Institute, School of Chemistry, Cardiff University, Park Place, Cardiff CF10 3AT, UK

Email: kamalchem.roy@gmail.com, drdebashree@biet.ac.in

Abstract:

A novel folic acid-conjugated composite nanoparticle containing Cu on TeO_2 (FA-NC) was developed via a green synthetic route for targeted cancer theranostics. The nanocomposite exhibited strong fluorescence, enabling sensitive detection of folate receptor-positive HeLa cells with a detection limit of 1.82×10^3 cells/mL. XPS analyses confirmed the transformation of Cu^{2+} to Cu^0, and successful surface modification with folic acid was confirmed using Raman spectroscopy. The nanocomposite demonstrated selective imaging of HeLa cells over HaCaT cells, confirming receptor-specific targeting. Furthermore, FA-NC exhibited antiproliferative activity towards HeLa cells with an IC_{50} of 15 µg/mL. A moderate DNA binding affinity (K_d = 69.2 µM) suggested groove-binding interaction. These results highlight FA-NC as a cost-effective, biocompatible, and dual-functional nanomaterial for simultaneous imaging and therapy of folate receptor-positive cancer cells.

Keywords: Theranostic; cancer cell imaging; fluorescence microscopy; antiproliferative property

Dedicated to Professor Debashis Ray, celebrating a career in Inorganic Chemistry.

1. Introduction

Cancer is the second most reason behind premature fatality over the globe. Cancer diagnosis still remains extremely challenging owing to a difficult to achieve effective differentiation between cancer and normal cells. The circulating tumor cells (CTC) flow through the blood stream to form a new metastasis and hence ultra-trace detection of CTCs is considered as early diagnosis of cancer in order to increase the survival rate of the patients suffering from cancer [1, 2].

Commonly used cancer detection techniques include tissue biopsy and other medical imaging methods like Magnetic Resonance Imaging (MRI), Single-photon Emission Computed Tomography (SPECT), Positron Emission Tomography (PET), etc. [3]. These techniques are applicable only upon delocalization of the cancer cells from the primary site to different parts of the body (metastasis) where the circulating tumor cells get accumulated [4]. These techniques require a quite high concentration of cancer cells for detection, which means they have lower sensitivity of detection, in spite of their high cost. Cancer can be effectively treated if diagnosed at an early stage. Fluorescence imaging technique can serve as an effective tool to serve the purpose of fast diagnoses [5]. Several fluorescent dyes are available for the detection of cancer cells, but many of these dyes have major drawbacks as they suffer from extensive photo-damage, high toxicity and low water solubility [6]. Nanoparticles are found to aid in efficient ultra-trace detection of cancer cells [7]. Hence, exploring their optical properties to use in the bioimaging arena may lead to breakthrough developments in cancer detection and treatment. Surface functionalization of nanoparticles using different biomolecules (including biomarkers) has proved to be highly effective in cell imaging [8].

The two major classes of nanoparticles with tunable optical absorption in the near-infrared region are noble metals and semiconductor nanoparticles. Gold nanoparticles of various shapes, such as gold nanoshells, gold nanorods, gold nanocages and hollow gold nanospheres have been explored extensively for biomedical applications, especially bioimaging [9]. However, several factors like complicated and high cost of synthesis, non-degradability, and strong dependence on the dielectric function of the surrounding medium are problems faced in their further development. An alternative to noble metal-based nanoparticles is copper-

based chalcogenide semiconductor nanoparticles. The absorption and fluorescence properties of semiconductor nanoparticles originate from their quantum confinement effect [10].

Surface modifications and biofunctionalization make these nanoparticles highly applicable in the biomedical field. The folate–folate receptor (FA–FR) axis has been extensively explored as a molecular targeting strategy owing to the overexpression of FRs on various malignant cells and minimal expression in most normal tissues. Due to its good stability, compatibility with both organic and aqueous solvents, and high affinity towards folate receptor ($K_d \approx 10^{-10}$ M), folic acid is the perfect ligand for FR and thereby actively targeting tumor tissues [11, 12]. Numerous studies have employed FA conjugation to achieve selective imaging and therapy. For example, FA-functionalized quantum dots have been developed for fluorescence imaging of FR-positive cancer cells [13, 14], while FA-linked organic fluorophores and nanocarriers have enabled enhanced tumor-specific imaging and drug delivery [15, 16]. Carbon nanodots were conjugated with folic acid and used for targeting and detecting cancer cells in a mixture of NIH-3T3 and HeLa cells [11]. More recently, FA-conjugated metal-based nanomaterials and polymeric materials have demonstrated efficient dual imaging and therapeutic performances [12, 17, 18]. For instance, FA-conjugated AuNCs@SiO_2 nanoprobes have been developed for fluorescent and X-ray computed tomography imaging of FR (+) MGC-803 cells (human gastric carcinoma cell line) [19]. Wen et al., have developed β-cyclodextrin (β-CD) polymer conjugated with FA, which further forms inclusion complexes with indocyanine green (ICG) (ICG@PCD-FA) [12]. This ICG@PCD-FA has shown a targeted impact on HeLa cells that were positive for the folate receptor (FR+). These reports collectively establish FA–FR targeting as a well-validated approach in nanotheranostics.

In this study, a fluorescent nanoparticle, consisting of copper and copper tellurite ($CuTeO_3$) was conjugated with folic acid and used for selective and specific detection of human cervical cancer cell line HeLa. A green synthetic approach was followed for the preparation of the nanocomposite of copper on copper tellurite (CuTe-NC) from aqueous solution of potassium tellurite and copper sulphate in presence of ascorbic acid. The surface of the CuTe-NC nanoparticles was modified by folic acid to have the specificity towards folate receptor positive cancer cells. Fluorescence based microscopic and spectroscopic experiments confirmed the sensing ability of folic acid conjugated nanoparticles towards CTCs. The interaction of folic acid with CuTe-NC eventually leads to the formation of FA-NC

nanocomposite. The interaction of the nanocomposite with CTCs was studied using fluorescence spectroscopy which validated the mechanism of sensing capability of FA-NC nanocomposite towards CTCs. The antiproliferative property of FA-NC nanocomposite was further investigated to explore its theranostic application. In addition to that, the binding property of nano FA-NC with DNA was established using fluorescence, isothermal calorimetry, circular dichroism and theoretical study to validate its therapeutic potency. The study unravels the novel property of FA-NC nanocomposite as a DNA probe. The novelty of this work lies in the development of a folic acid–conjugated nanocomposite synthesized via a green route that combines fluorescence sensing, folate receptor-specific cell imaging, and therapeutic cytotoxicity in a single biocompatible platform. Unlike organic dye–based or polymeric nanocarriers, FA-NC itself is fluorescence active, enabling label-free visualization and selective killing of folate receptor–positive cancer cells. The present study uniquely introduces FA-NC, where folic acid not only acts as a targeting ligand for folate receptor–positive cancer cells but also reduces Cu^{2+} to Cu^{0} and offers fluorescence activity. This synergistic design integrates diagnostic (fluorescence imaging and sensing) and therapeutic (DNA interaction and cytotoxicity) functionalities in one biocompatible nanocomposite, establishing a new platform for low-cost cancer theranostics.

2.1. Materials

Copper sulphate, potassium tellurite, ascorbic acid, folic acid (FA), BDNA, and potassium bromide were procured from Sigma India. Chinese hamster ovary cells CHO and human cervical cancer line HeLa were purchased from ATCC. Trypan blue was procured from Sigma Aldrich. Dulbecco's modified Eagle medium (DMEM), penicillin, streptomycin, fetal bovine serum (FBS), trypsin-EDTA solutions were obtained from HiMedia. Dichlorofuoroscein diacetate (H_2DCF-DA) was obtained from Calbiochem of Merck-Millipore (Billerica, MA, United States).

2.2. Instrumentation

Transmission electron microscope (TEM) (JEOL JEM-2100F) was used to record the images and selected area electron diffraction (SAED) patterns of CuTe-NC and FA-NC nanocomposite. Malvern Zetasizer Nano instrument for dynamic light scattering (DLS) and zeta potential measurement experiments. A Rigaku SmartLab automatic high resolution

multipurpose PC Controlled X-Ray diffractometer system was used for powder X-ray diffraction (PXRD) analysis. Fourier transformed infrared (FT-IR) spectroscopic analysis was performed using a Perkin-Elmer instrument. Labman digital ultrasonic cleaner (model: LMUC-2, sonication power 100 W) for sonication and Remi Elektrotechnik Ltd R-4C centrifuge for centrifugation were used. The fluorescence measurements were performed using a Hitachi spectrophotometer and Raman spectral measurements were carried out using Reneshaw inVia Raman microscope equipped with 50X lens. Thermo Evos M5000 instrument was used for fluorescence microscopic experiments. A Kratos Axis Ultra DLD system was used to collect XPS spectra using monochromatic Al Kα X-ray source operating at 140 W (10 mA × 14 kV). Data was collected with pass energies of 160 eV for survey spectra, and 20 eV for the high-resolution scans with step sizes of 1 eV and 0.1 eV respectively. Samples were either pressed on to doubled sided Scotch tape (type 665) attached to a glass slide. The system was operated in the Hybrid mode, using a combination of magnetic immersion and electrostatic lenses and acquired over an area approximately 300×700 μm^2. A magnetically confined charge compensation system was used to minimize charging of the sample surface, and all spectra were taken with a 90 ° take of angle. A base pressure of ~ 5×10^{-9} Torr was maintained during collection of the spectra. Data was analysed using CasaXPS (v2.3.27PR4.4) after subtraction of a Shirley background and using modified Wagner sensitivity factors as supplied by the manufacturer. Flow cytometric assessment was carried out using a BD FACS Calibur (Becton Dickinson, NJ, US) flow cytometer equipped with a 488 nm excitation laser and a 530 ± 30 nm bandpass filter (FL1 channel). The data were analyzed with FlowJo software. Circular dichroism (CD) spectroscopy was performed using Jasco J1100 model.

2.3. Synthesis and Characterization of CuTe-NC

To 5 mL (50 mM) aqueous solution of $CuSO_4$, 10 mL of 20 mg/mL ascorbic acid solution and 5 mL (50 mM) aqueous solution of K_2TeO_3 were added simultaneously followed by vigorous mixing using magnetic stirrer for a few minutes. The solution was then allowed to stand for 2 h at room temperature. Dark brown nanoparticles appeared which were washed with distilled water for 2 to 3 times and were dried under IR lamp (Figure 1). The particle size was confirmed by TEM. The hydrodynamic radius was estimated by dynamic light scattering experiment. The band-gap of the nanoparticles was determined by UV-Visible spectroscopy.

The functional groups present on the surface of the nanoparticles were analysed by FTIR and Raman spectroscopic measurements. Powder X-ray diffraction (PXRD) was carried out to determine the pattern of the crystal lattice. The elemental composition and the redox state of the elements present in the nanocomposite were determined by XPS study.

Figure 1: Schematic diagram for synthesis of UNC

2.4. Synthesis and Characterization of FA-NC

The FA-NC nanocomposite was prepared by further conjugation of CuTe-NC nanocomposite with FA for increasing selectivity and specificity towards cancer cells. At first, isothermal calorimetric titration was carried out to determine the thermodynamic parameters and binding stoichiometry for the interaction between CuTe-NC and folic acid. To modify the surface of CuTe-NC nanocomposite with folic acid, one tablet of folic acid (5 mg) was dissolved in 5 mL of 3.7 mg/mL Na_2CO_3. The solution was centrifuged at 10,000 rpm for 15 min. 3 mL of the supernatant solution was added to 1 mg of dried CuTe-NC nanocomposite. The resulting mixture, containing 0.1% (w/w) FA, was kept on a shaker overnight (Figure 2). The nanocomposite solution was then taken for characterization using TEM, DLS, FTIR and Raman spectroscopy to confirm the surface modification.

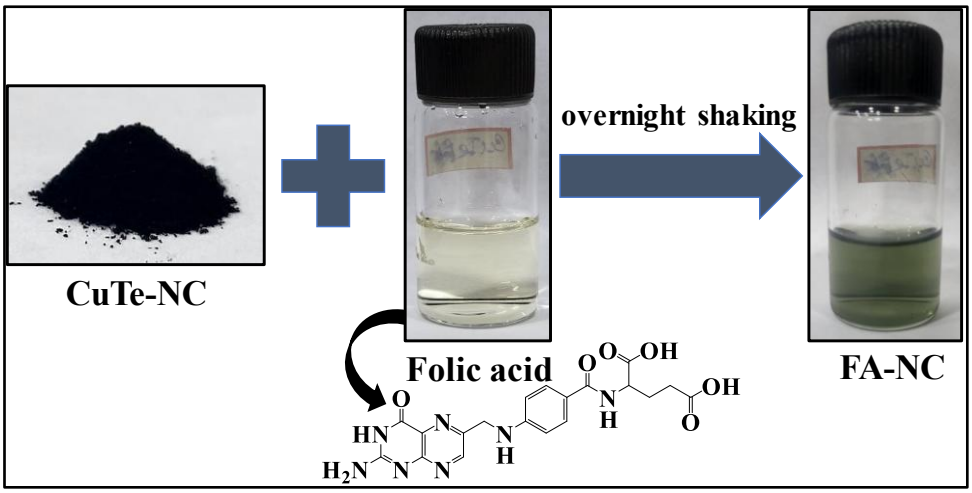

Figure 2: Schematic diagram for synthesis of CNC

2.5. Quantum Yield (QY) Calculation of FA-NC

Using Rhodamine B in water as a reference dye, the fluorescence QY of FA-NC in water was determined using the following equation [20] at an excitation wavelength of 400 nm.

$$QY_{FA-NC} = QY_R \times \left(\frac{A_R}{A_{FA-NC}}\right) \times \left(\frac{F_{FA-NC}}{F_R}\right) \times \left(\frac{n_{FA-NC}}{n_R}\right)^2 \quad (1)$$

where QY is the fluorescence quantum yield, F is the observed integrated fluorescence intensity, A is the absorbance of the solution at the excitation wavelength, and n is the refractive index of the solvent. The subscripts "R" and "FA-NC" stand for the reference (Rhodamine B, QY=0.31 in water) and the sample, respectively.

2.6. Determination of Photostability of FA-NC

The photostability of FA-NC was investigated by monitoring the change in fluorescence intensity with irradiation time under UV light. To examine the photostability of FA-NC, the sample was continuously exposed to UV light (365 nm) for four hours, and the fluorescence intensity was periodically monitored.

2.7. Cell Culture

The folate receptor (FR) negative Chinese hamster ovary cells, CHO and FR positive human cervical cancer line HeLa were maintained in DMEM high glucose medium, supplemented with 1% penicillin-streptomycin, and 10% FBS. Upon reaching 90% confluency, the cells were trypsinized with 0.25% trypsin-EDTA solution and distributed in 3 flasks for future use. All the cells were kept at 37°C in a CO_2 incubator that maintains 5% CO_2 pressure. Human keratinocyte cell line, HaCaT (normal cells) was grown in DMEM media supplemented with 10% FBS and 1% penicillin-streptomycin at 37°C in 5% CO_2 environment.

2.8. Fluorometric Detection of Cancer Cell

The fluorescence property of FA-NC nanocomposite was explored to investigate its capacity as a microscopic as well as a spectroscopic sensor towards folate receptor positive cancer cells.

2.8.1. Fluorescence Microscopic Imaging

Cell imaging experiments were carried out using a fluorescence microscope (Thermo Evos M5000). HaCaT and HeLa cells (~1×10^6) were cultured on cover slips and the cells were treated with 5 µg/mL concentration of FA-NC nanocomposite at 37°C for different time intervals. The untreated cells were considered as control. The treated cells were first washed thrice with PBS and then three times using 0.2% phosphate buffered saline with Tween 20 (PBST). Then, the cells were subjected to fixation for an hour at 4°C in 4 % paraformaldehyde. The treated cells were examined using fluorescence microscope.

2.8.2. Fluorescence Spectroscopic Study

Besides the imaging capability of FA-NC nanocomposite towards HeLa cells, its sensing ability was further checked by fluorescence spectroscopy. The fluorescence emission intensity of FA-NC nanocomposite was measured at 400 nm excitation wavelength with 5 nm slit widths for both excitation and emission channels using a 1 cm path length quartz cuvette. The changes in emission intensities of FA-NC nanocomposite were recorded due to successive addition of small aliquots of the media containing the cancer cells. The baseline

corrected fluorescence intensity values were plotted against the cell count. From this plot, the Limit of Detection (LOD) was calculated according to the equation [21]:

$$\mathrm{LOD} = 3.3 \times \frac{\text{standard deviation}}{\text{slope}} \quad (2)$$

2.9. Cellular Uptake Analysis by Flow Cytometry

To understand the role folic acid receptor both folic acid unconjugated and conjugated nanocomposites (CuTe-NC and FA-NC) were used to treat the HeLa cells. Out of the two NCs, only FA-NC showed uptake in HeLa cells presumably due to its FR +ve nature. Therefore, to further cross check the mutual compatibility of FR+ cells and FA-NCs, the uptake of FA-NCs by FR –ve CHO cells were also studied. 1×10^6 cells of both HeLa and CHO were seeded in six-well plates individually. The medium containing CuTe-NC and FA-NC (5 µg/ mL) were added separately in each well. After 4-6 h of incubation, cells were washed with phosphate-buffered saline (PBS, pH 7.4) 3 times to remove unbound nanocomposites, detached using trypsin-EDTA, and resuspended in PBS for analysis. Again, the cellular uptake efficiency of FA-NCs were quantitatively assessed by flow cytometry using FR –ve (CHO) cell lines. The seeded cells were incubated overnight to reach a good confluence. Subsequently, the cells were treated with FA-NC nanocomposite (5 µg/mL) for 4-6 h at 37 °C to check if there was any kind of endocytosis. Forward scatter (FSC) and side scatter (SSC) parameters were used to gate the viable single-cell population, while fluorescence histograms were generated to quantify nanocomposites internalization.

2.10. Cell Viability Assay

To check the effect of CuTe-NC and FA-NC on cancer cells, Cell viability assay was done using HeLa cell line by MTT assay [22]. 1×10^4 cells were seeded in 96 well plate. After 24 h of cell seeding, the cells were treated with different concentrations of CuTe-NC and FA-NC nanocomposites (0-50 µg/mL) and the treated cells were incubated for 48 h. After incubation, 10 µl of MTT (5 mg/mL stock solution) was added to 100 µL of medium. The plate was then incubated at 37 °C for 3 h. The medium was removed and DMSO was added to dissolve the formazan crystal. The absorbance was taken at 570 nm. The cell viability was expressed in percentage (%).

2.11. Intracellular ROS Generation using Flow Cytometry

To evaluate intracellular reactive oxygen species (ROS) generation induced by the nanocomposites, the cell-permeable probe H_2DCFDA was used. Once internalized, endogenous esterases deacetylate H_2DCFDA to non-fluorescent H_2DCF. This H_2DCF is subsequently oxidized by hydrogen peroxide or other low-molecular-weight peroxides to form the highly fluorescent 2′,7′-dichlorofluorescein (DCF). HeLa cells (1×10^6) were seeded in six-well plates and treated with CuTe-NC or FA-NC. The ROS production in HeLa cells was measured by flow cytometry with CuTe-NC and FA-NC nanocomposites using their LD_{50} values (lethal dose 50, dose of the nanocomposites that is lethal to 50% of cell population). After 2 h of incubation, the cells were harvested by trypsinization, washed with PBS, and incubated with 3 mM H_2DCFDA for 15 min at 37 °C in the dark [23]. DCF fluorescence was quantified using flow cytometry (FL1-H channel), and the mean fluorescence intensity was used as a measure of intracellular ROS levels.

2.12. Assessment of Mitochondrial Membrane Potential (MMP)

Mitochondrial membrane potential (ΔΨm) was evaluated using a JC-1 dye–based flow cytometric assay following standard protocols widely applied for assessing mitochondrial integrity in apoptotic studies. JC-1 usually forms red-fluorescent aggregates in mitochondria and comes out to cytosol as green-fluorescent monomers under conditions of mitochondrial depolarization due to adjustment of membrane potential. HeLa cells (1×10^6) were seeded in six-well plates and treated with CuTe-NC or FA-NC nanocomposites for 2 h in order to detect the change in membrane potential. HeLa cells which were not treated with nanocomposites were served as the control. All the treated and untreated cells were trypsinized after 3 h and resuspended in JC-1 solution (2.5 µg/mL) and incubated for 20 min at 37 °C in the dark [23]. After staining, the fluorescence of the cells was measured at 525 and 590 nm using a flow cytometer.

2.13. DNA Binding Study

2.13.1. Fluorescence Study

To understand the DNA binding ability of nano FA-NC, fluorescence spectroscopic study was performed using a PerkinElmer LS-55 fluorescence spectrometer to investigate the mode of

interaction between FA-NC nanocomposite and DNA. The intrinsic emission spectra of FA-NC nanocomposite were recorded with excitation maxima at 400 nm keeping both excitation and emission slit at 5 nm and using the cuvette of path length 1 cm. A series of known aliquots of DNA, concentrations ranging between 0-60 μM, were added successively to the working solution of FA-NC nanocomposite (2 μg/mL) and the changes in fluorescence intensities were recorded.

2.13.2. Isothermal Titration Calorimetry (ITC)

To understand the molecular basis and forces involved in the interactions between FA-NC nanocomposite and DNA, isothermal calorimetric titration was performed using Malvern PeaqITC Microcal instrument. The thermodynamic parameters associated in this interaction are determined using the equation below [24]:

$$\Delta G = \Delta H - T\Delta S \quad (3)$$

In this equation, ΔG stands for Gibbs free energy, ΔH for change in enthalpy, ΔS for change in entropy, and T for absolute temperature. The blank experiments were carried out in order to remove the background effects from the studies.

2.13.3. CD Spectroscopic Study

The CD spectra of the DNA (25 μM) in 5 mM phosphate buffer, pH 7.4, was recorded in far UV range of 200–300 nm using a quartz cell of 1 mm path length. The changes in secondary structure of DNA in presence of FA-NC nanocomposite at two different concentrations were also recorded to find out the DNA structure modulating ability of the nanocomposite (if any). All the spectra were recorded as an average of three runs and corresponding blank experiments were carried out for base line correction.

2.13.4. Theoretical Study

A theoretical model of FA-NC nanocomposite was built using Avogadro software. The theoretical interaction between the nanoparticles and B-DNA strand (PDB ID:453d) were

determined using Hex 8.0 software [25]. The energy minimized docked complexes were visualized by PyMol software.

3. Results and Discussions

3.1. Characterization of CuTe-NC and FA-NC Nanocomposite

Transmission electron microscopic (TEM) images were recorded to determine the size, surface morphology and size distribution of the nanocomposite. Figure 3 (A, B) shows the TEM images of CuTe-NC and FA-NC nanocomposite respectively. Both the nanocomposites are found to have spherical shape with average diameter of ~5 nm. The FA-NC generated a lighter shade compared to the CuTe-NC because of the presence of folate conjugation. Figure 3 (C, D) present the corresponding SAED images of CuTe-NC and FA-NC nanocomposites respectively, showing microcrystallinity of both the nanocomposite.

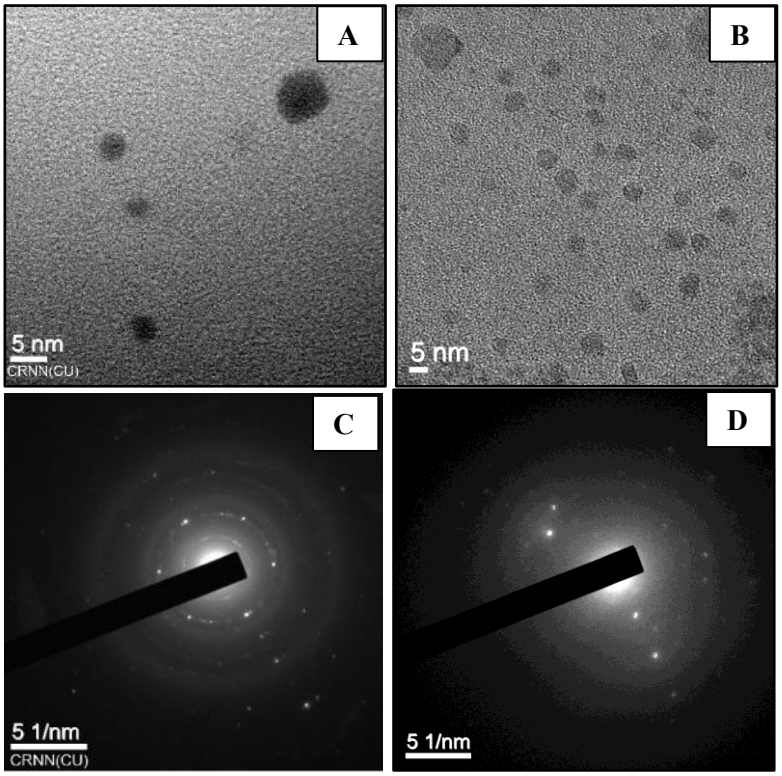

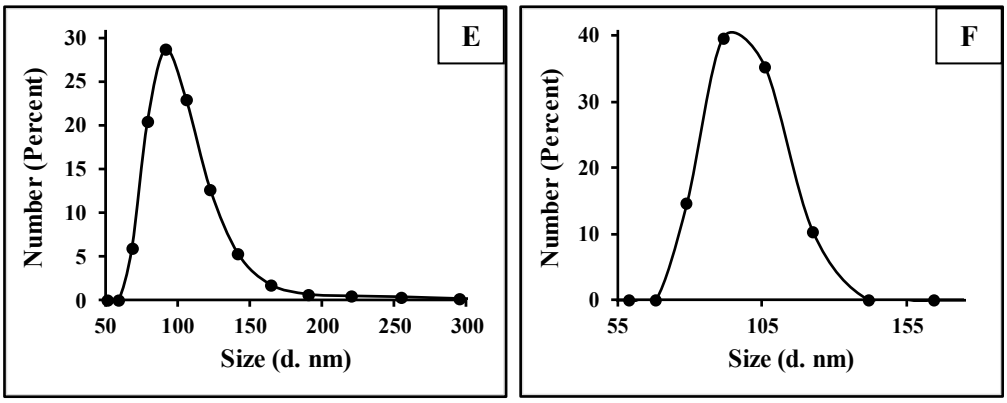

Figure 3: (A) TEM image of CuTe-NC nanocomposite; (B) TEM image of FA-NC nanocomposite; (C) SAED pattern of CuTe-NC nanocomposite; (D) SAED pattern of FA-NC nanocomposite; (E) Hydrodynamic radius of CuTe-NC nanocomposite; (F) Hydrodynamic radius of FA-NC nanocomposite.

The hydrodynamic radii of CuTe-NC and FA-NC nanocomposites can be seen from Figure 3E and 3F respectively. The larger particle size shown by DLS as compared to that shown by TEM images is quite obvious because of the hydrodynamic radius as measured by DLS in solution state. The size difference between TEM and DLS measurements can be explained by a subtle reorganization of the nanocomposites in the hydration environment. Table 1 show zeta potential values of CuTe-NC and FA-NC nanocomposites which are -26.16 mV and -35.7 mV respectively. The high zeta potential values of the nanocomposites suggest that they are electrically stabilized, sterically protected to a good degree, and less likely to agglomerate quickly [26]. In case of FA-NC nanocomposites, higher negative zeta potential value arises due to presence of carboxyl groups present in folic acid. This higher –ve zeta potential value of FA-NC also accounts for its better stability avoiding aggregation and more suitability for fluorescence imaging.

Table 1: ζ potential values of CuTe-NC and FA-NC

Variation	Zeta potential (mV)
CuTe-NC	-26.6
FA-NC	-35.7

Powder X-ray diffraction pattern obtained for nano CuTe-NC is as shown (Figure 4). Comparing the peaks with the database obtained from Joint Committee on Powder Diffraction Standards (JCPDS), possible (hkl) planes were assigned as shown in Table 2. The highest intensity peaks in CuTe-NC (for 2θ = 27.43 and 29.32, denoted in the figure with blue and red arrows respectively) correspond to an orthorhombic system. Upon the modification of CuTe-NC with FA, the diffraction pattern of the resulting FA-NC changes and appearance of different new peaks are observed. Major diffractions appear due to 2θ values of 27.55°, 30.07°, 34.47°, 35.19°, and 37.93° which corresponds to (102), (022), (221), (321), and (400) respectively. The lattice system of FA-NC is mostly orthorhombic.

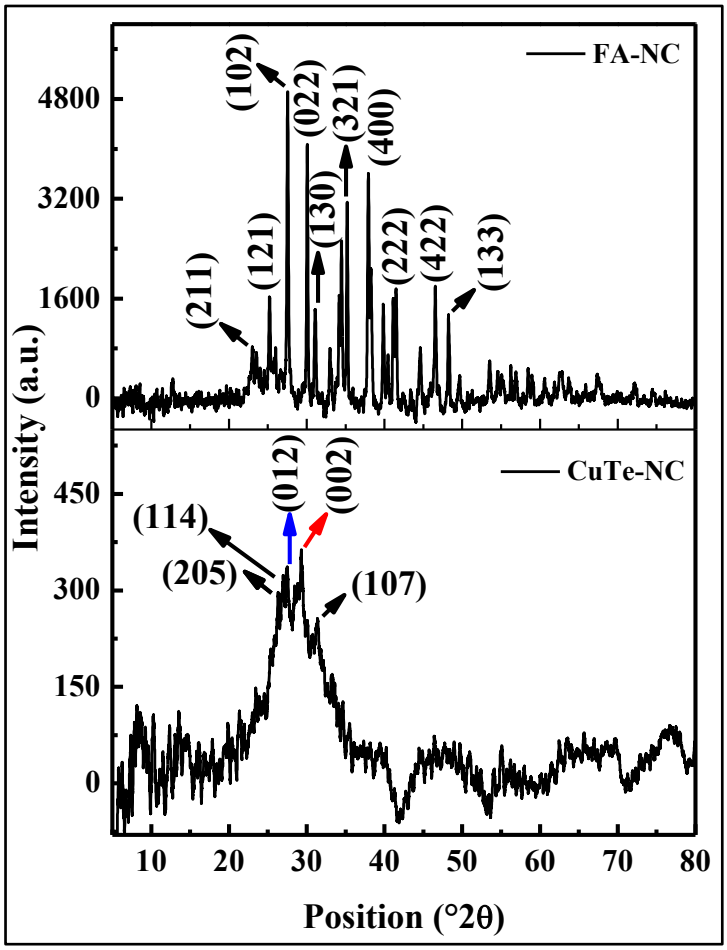

Figure 4: PXRD pattern for CuTe-NC and FA-NC.

Table 2: PXRD data of CuTe-NC and FA-NC with possible assignment of JCPDS number

Serial no.	Observed position (2θ)	Database (2θ)	hkl Plane	Possible system	JCPDS no.
CuTe-NC					
1.	26.34	26.299	205	Hexagonal	530524
2.	26.99	26.932	114	Hexagonal	831320
3.	27.43	27.408	012	Orthorhombic	892053
4.	29.32	29.256	002	Orthorhombic	270195
5.	31.43	31.485	107	Hexagonal	831320
FA-NC					
1.	23.01	22.842	211	Cubic	210881
2.	25.21	25.803	121	Orthorhombic	170733
3.	27.55	27.594	102	Orthorhombic	170733
4.	30.07	30.378	022	Orthorhombic	170733
5.	31.11	31.027	130	Orthorhombic	170733
6.	34.47	35.023	221	Orthorhombic	170733
7.	35.19	35.193	321	Cubic	210881
8.	37.93	37.703	400	Cubic	210881
9.	39.86	39.655	132	Orthorhombic	170733
10.	41.11	41.011	222	Orthorhombic	170733
11.	46.52	46.611	422	Cubic	210881
12.	48.23	48.459	133	Orthorhombic	170733

The oxidation state and composition of the elements present in the nanocomposite were obtained from the XPS spectra and the corresponding results are summarized in table 3 and figure 5 and 6. It was found that the total atomic % of Cu in CuTe-NC nanocomposite was ~8.5, with the spectra indicating the presence of both Cu(0) and Cu^{2+} based on the binding energies (932.8 and 934.7 eV respectively), with the shape of the Cu^{2+} shake-up structure suggesting both CuO and some $Cu(OH)_2$. The total atomic % of Te was ~11%, with binding energies for the Te $3d_{5/2}$ state indicative of Te oxide, a small amount of hydroxide and metallic (likely alloy) Te [27].

On conjugation of folic acid with the CuTe-NC nanocomposite, the resultant FA-NC nanocomposite is now found to have modified where Cu is entirely present in its pure metallic form, however as shown in figure 6, the $Cu2p_{3/2}$ peak is significantly smaller, suggesting attenuation of the signal due to the organic overlayer. A deeper analysis of the data reflects the probable reason of high potential of FA-NC nanocomposite over CuTe-NC nanocomposite in terms of their theranostic application. In case of CuTe-NC nanocomposite, copper is mostly present in +2 oxidation state (~74%) and metallic copper (Cu^0) is present in a smaller amount (~26%) (table 4). On the other hand, in FA-NC nanocomposite, folic acid facilitates the reduction of the entire copper from its +2 oxidation state to its metallic form (Cu^0 ~100%). Folic acid has earlier been used both as a surface ligand and as a direct reducing/capping agent in one-pot green syntheses of metal nanoparticles, which corroborates with our study that FA can simultaneously functionalize and influence the Cu oxidation state during nanoparticle formation [28]. Cu^0 possesses excellent redox activity [29] (easily oxidizable) and can interact with biological enzymes. This property can be leveraged for imaging purposes and also shows higher therapeutic efficacy. It is noteworthy to mention that percentage shares of Te^{4+} (88%) and Te^0 (12%) in both CuTe-NC and FA-NC nanocomposite remain somewhat unaltered before and after folic acid conjugation. This further establishes that increase in % Cu^0 in FA-NC nanocomposite is the key factor which sets these nanocomposites apart from its unmodified counterpart CuTe-NC for their biological application. Also, the Te:Cu ratio is modified from 1.3:1 (in CuTe-NC nanocomposite) to 5.2:1 (in FA-NC nanocomposite). Nonetheless, in FA-NC nanocomposite, total atomic % of carbon (1s) increased to a larger extent (65.81%) which comes from the contribution of carbon chains present in folic acid.

Table 3: XPS derived atomic percentages of elements present in the nanocomposite. Where binding energies are given, these are for the primary photoelectron signal for a particular oxidation state (e.g. Cu^{2+})

Sample	Elements	Position (eV)	Atomic %	Sample	Elements	Position (eV)	Atomic %
CuTe-NC	Cu $2p_{3/2}$ Metallic	932.8	2.28	FA-NC	Cu $2p_{3/2}$ Metallic	932.7	0.05
	Cu $2p_{3/2}$ (Cu^{2+})	934.7	6.34		Te $3d_{5/2}$ Alloy	572.3	0.06
	Te $3d_{5/2}$ (Oxide)	576.6	8.96		Te $3d_{5/2}$ (Oxide)	576.4	0.15
	Te $3d_{5/2}$ (Hydroxide)	577.7	0.66		Te $3d_{5/2}$ (Defective oxide)	574.3	0.05
	Te $3d_{5/2}$ (Alloy)	573.2	1.37		O 1s	531.41	9.33
	O 1s	531.1	36.96		O 1s	532.92	18.88
	C 1s	285.0	20.92		C 1s	285.0	33.97
	C 1s	286.4	14.33		C 1s	286.5	21.78
	C 1s	288.8	7.84		C 1s	289.6	3.16
	S 2p (SOx)	168.9	0.36		C 1s	288.2	6.9
					N 1s	399.5	1.82
					Na 1s	1071.49	3.83
					Cl 2p	198.3	0.11

Table 4: Comparison of atomic percentage of elements present in the nanocomposites

Nanocomposite	Atomic % of elements			
	Cu^{2+}	Cu^{0}	Te^{4+}	Te^{0}
CuTe-NC	74	26	88	12
FA-NC	0	100	88	12

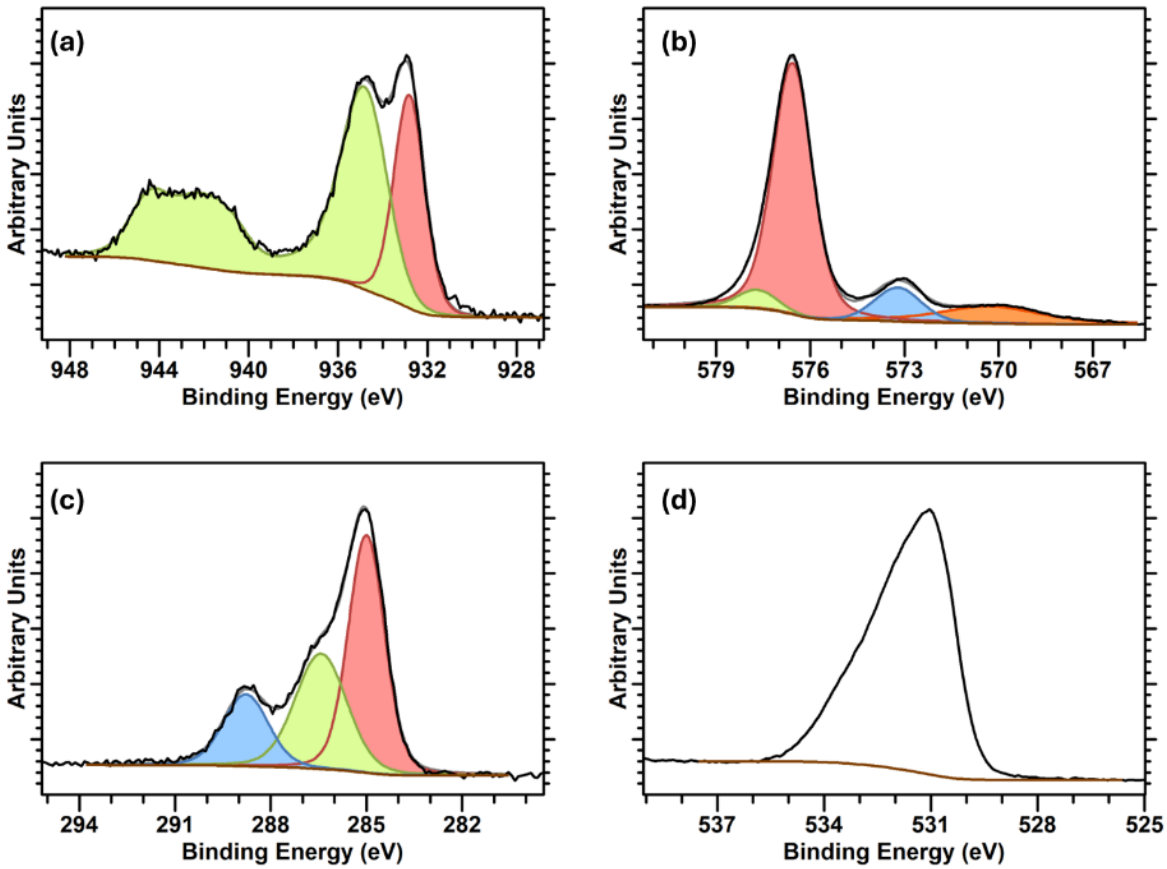

Figure 5: (a) $Cu2p_{3/2}$, (Green = Cu(II) and Red = Cu(0)) (b) $Te3d_{5/2}$(Red = TeO_2, Blue = Te(0) and green = hydroxide), the orange peak is a structure from the Cu Auger signal), (c) C1s (Red = C-C/C-H, Green = C-O functions, blue = COO functions) and (d) O1s (unfitted) spectra of CuTe-NC nanocomposite.

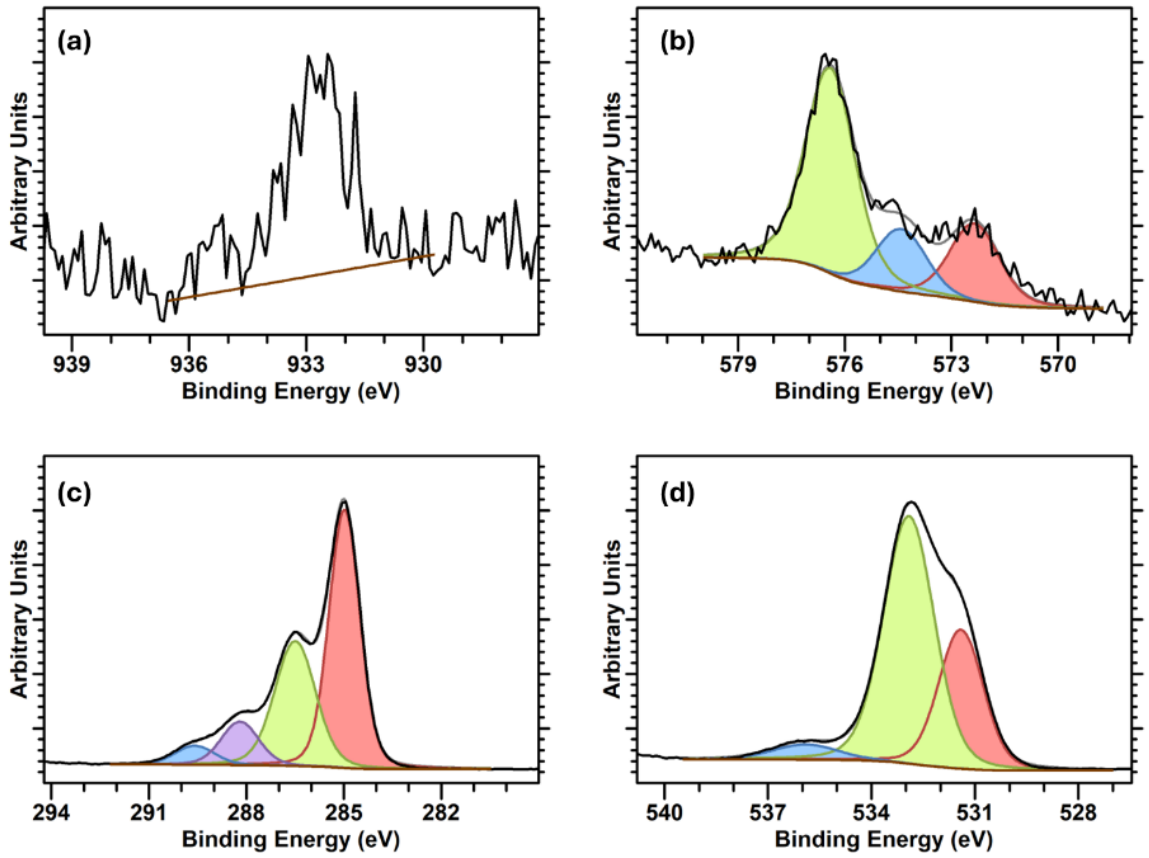

Figure 6: (a) Cu2p$_{3/2}$, (b) Te3d$_{5/2}$, (c) C1s (Red = C-C/C-H, Green = C-O functions, purple = C=O functions, blue = COO functions) and (d) O1s (Red = oxide/hydroxide and organic, green = C-O functions and blue = Na Auger) of FA-NC nanocomposite.

Raman spectra of CuTe-NC and FA-NC nanocomposite are shown in figure 7 and table 5 summarizes the different peak positions with corresponding functional groups present on the surface of the nanocomposite. The Raman spectra for CuTe-NC nanocomposite gave a characteristic peak at 125 and 144 cm^{-1} corresponding to Te-O bond vibration (figure 7), which agrees with that of the Raman spectra of α-TeO_2 [30]. While figure 8 shows the presence of multiple peaks, other than Te-O bond which confirms the surface modification of CuTe-NC nanocomposite in presence of folic acid. Figure 8 shows the presence of absorption bands at 2900 cm^{-1} due to C-H stretching, 1377 cm^{-1} for C-H rocking, 1339 cm^{-1} for C-H bending, 1262 cm^{-1} C=N rocking, 1081 cm^{-1} for C-O-C stretching.

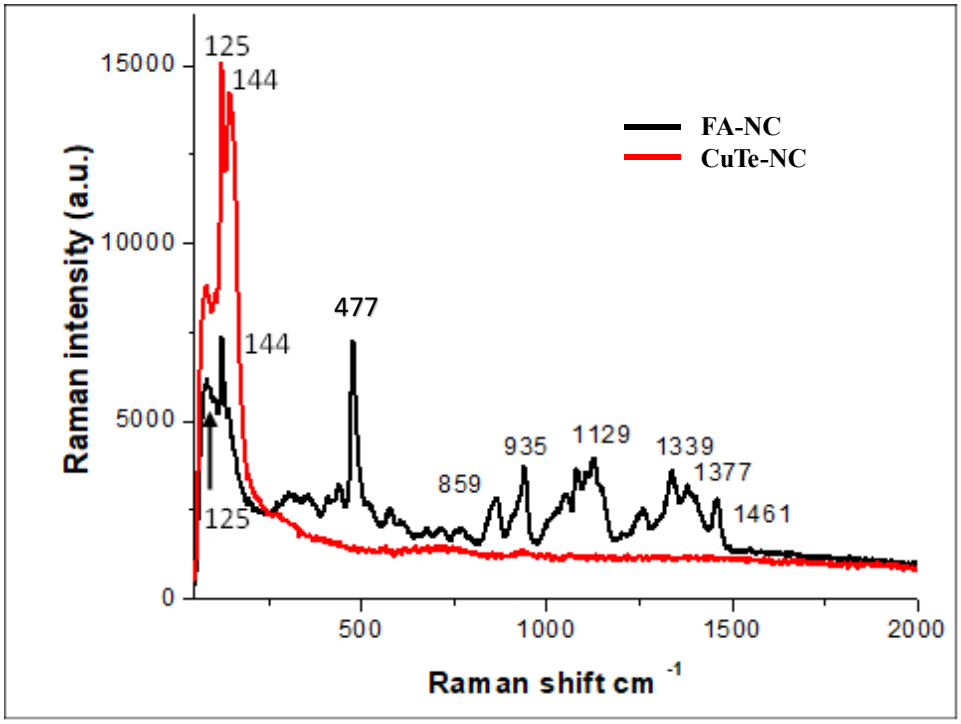

Figure 7: Raman spectra for CuTe-NC and FA-NC nanocomposite.

Table 5: Assignments for the characteristic Raman peaks

Serial no.	Peak position (cm^{-1})	Peak assignment
1	1461, 1377, 1339	C-H bending
2	1262	C=N rocking
3	1129	C-H bending
4	1081	C-O-C stretching
5	935, 859	C=C bending
6	477	Te-O-Te bending
7	125, 144	Te-O stretching

The synthesized FA-NC was found to exhibit intense fluorescence emission upon excitation at 400 nm. Table 6 enlists the parameters used for calculating the QY of FA-NC which has a value of 6.7%.

Table 6: Specific values of parameters for calculating QY of FA-NC

Sample	Integrated fluorescence intensity at λ_{em} = 454 nm (F) (a.u.)	Absorbance at λ_{ex} = 400 nm (A) (a.u.)	Refractive index of solvent (n)	Quantum Yield (QY)
Rhodamine B	500281	0.022	1.33	0.31
FA-NC	2023236	0.025	1.33	0.067

Figure 8 shows that even after four hours of UV exposure, FA-NC did not show significant loss in its original fluorescence intensity indicating good photostability.

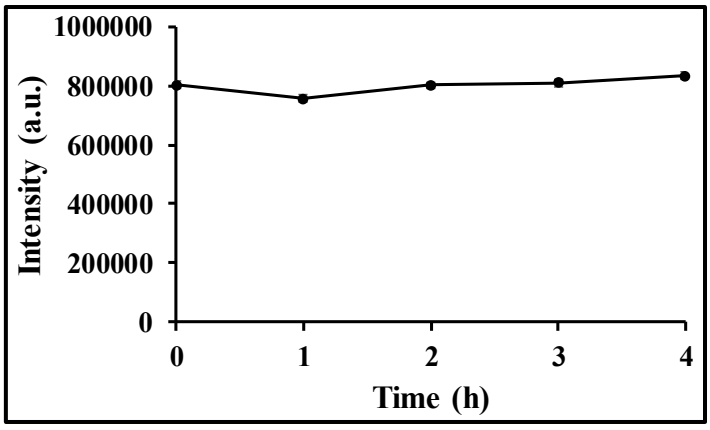

Figure 8: Photostability of FA-NC under continued irradiation with UV light (365 nm).

3.2. Selective Fluorescence Imaging of Cancer Cells using FA-NC

Figures 9a and 9b show the fluorescence microscopic bright field and green fluorescent images of HeLa cells respectively. Figure 10b shows green fluorescence signal from the surface of the cells due to binding of folic acid conjugated CuTe-NC nanocomposite (FA-NC) to the folate receptors present on the surface of the cancer cells. To confirm the specificity of FA-NC nanocomposite in binding with cancer cells, the same study was performed with HaCaT cells. Figures 9c and 9d show the fluorescence microscopic bright field and green fluorescent images of HaCaT cells, which shows very faint signal from the FA-NC nanocomposite, validating the selectivity of FA-NC nanocomposite towards folate receptor positive cancer cells. The physical state of the FA-NC nanocomposite (liquid) due to their low agglomeration tendency and higher interaction with the folate receptor containing cancer

cells make them the more suitable candidate for fluorescence imaging as compared to the CuTe-NC nanocomposite. Folate-conjugated nanoprobes are well documented to produce receptor-mediated uptake and improved selective imaging in folate receptor–overexpressing cells, which agrees with the selective HeLa imaging and sensing observed herein [31]. Folic acid functionalization of Cu-based nanostructures was also earlier shown to promote selective uptake into FR +ve HeLa cells, as FA-modified copper nanoclusters served both as reducers and targeting ligands to achieve imaging contrast between FR +ve HeLa versus folate FR -ve A549 cells [32].

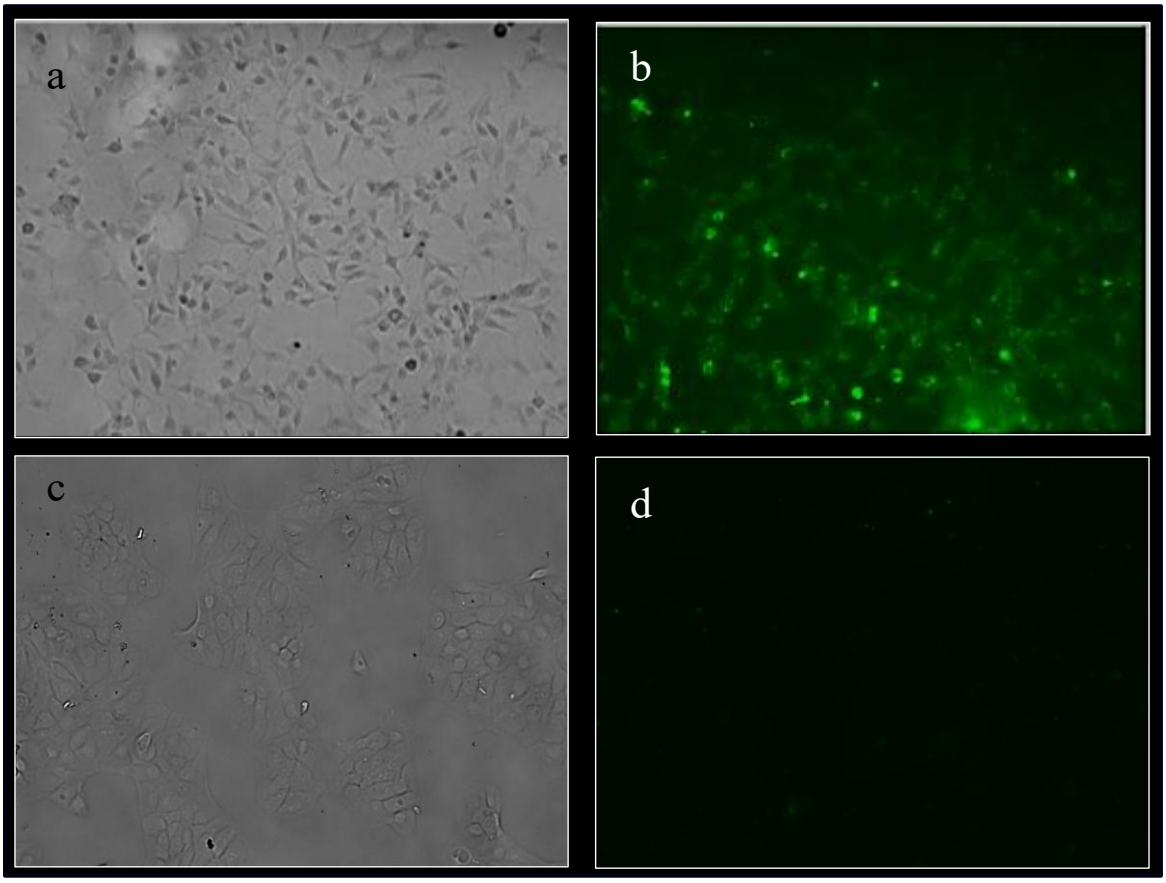

Figure 9: Fluorescence microscopic images of HeLa cells treated with 5 µg/ mL FA-NC shows (a) Bright field and (b) green fluorescence image; HaCaT cells treated with 5 µg/ mL FA-NC (c) Bright field, and (d) green fluorescence image.

3.3. Fluorescence Spectroscopic Detection of Cancer Cell using FA-NC

Spectroscopic sensing ability of FA-NC nanocomposite towards HeLa cells was further investigated to check its dual applicability as both fluorescence based microscopic and

spectroscopic sensor. The emission maximum of FA-NC nanocomposite was observed at 454 nm. The fluorescence intensity of FA-NC nanocomposite at this λ_{max} was found to increase with increase in cell count (Figure 10A). A plot of fluorescence intensity vs. cell count gave the LOD value of 1.82×10^3 cells (Figure 11B). The interaction between FA-NC nanocomposite and HeLa cells justifies the reason behind its ability towards selective both microscopic and spectroscopic detection of HeLa cells by FA-NC nanocomposite. The selective imaging of HeLa cells using FA-NC is in agreement with previous reports on FA-functionalized nanoprobes showing their receptor-mediated uptake in FR +ve cancer cells [33].

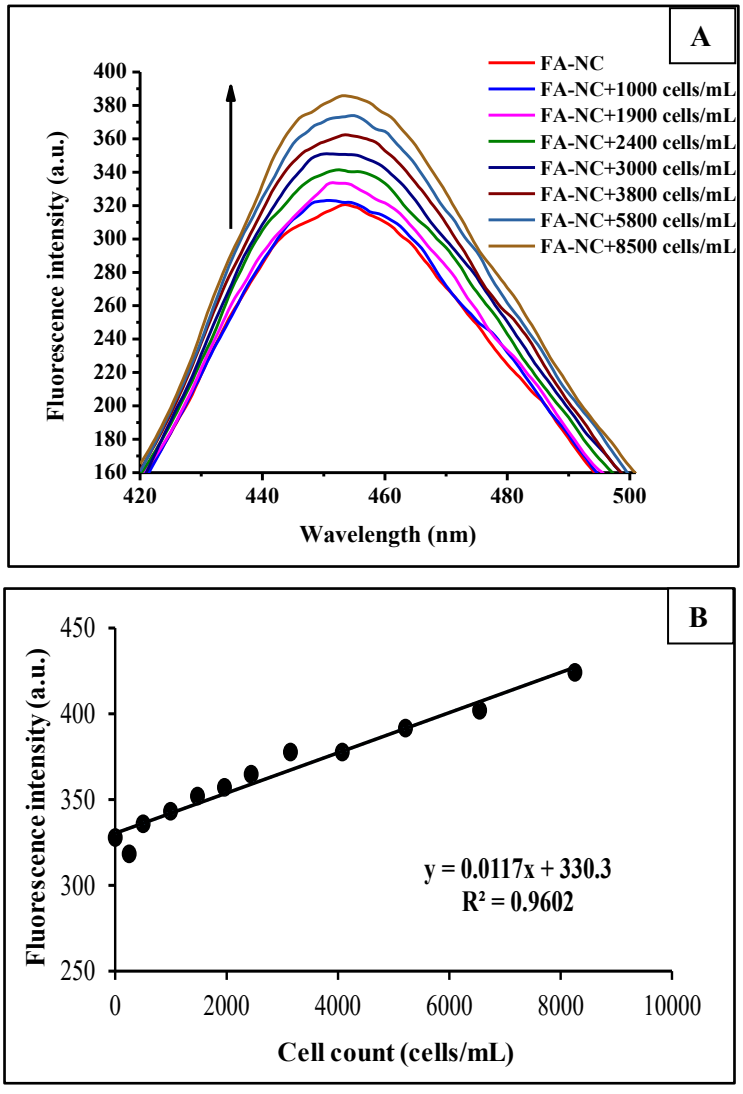

Figure 10: (A) Changes in emission spectra of FA-NC in presence of HeLa cells; (B) Calibration curve for the detection of HeLa cells by FA-NC.

3.4. Flow Cytometric Assessment of Receptor-Mediated Uptake

Flow cytometric evaluation revealed a pronounced enhancement in the fluorescence intensity in HeLa cells when exposed to FA-NC (Figure 11a and 11b) compared to unconjugated CuTe-NC nanocomposites (Figure 11c and 11d). The FA-NC nanocomposites exhibited a rightward shift in the fluorescence intensity histogram, with a mean intensity of 73.95±4.2, which is approximately double than that of the unconjugated CuTe-NC nanocomposites (35.64±2.7). This substantial increase in fluorescence intensity signifies effective internalization of the nanocomposites via folate receptor-mediated endocytosis (Figure 11b).

The HeLa cells treated with CuTe-NC nanocomposites displayed weak fluorescence with a lower median intensity, which arises primarily from nonspecific surface adsorption or passive diffusion. The distinct shift of the fluorescence peak from channel 29 (CuTe-NC) to channel 67 (FA-NC) strongly confirms that folic acid conjugation enhances the specificity and efficiency of cellular uptake in FR-positive HeLa cells. These findings demonstrate that functionalization with folic acid transforms FA-NC nanocomposites from nonspecific particles into a targeted delivery system capable of selective recognition and internalization by cancer cells overexpressing folate receptors. Figure 11e shows comparison in fluorescence intensity for various treatment conditions.

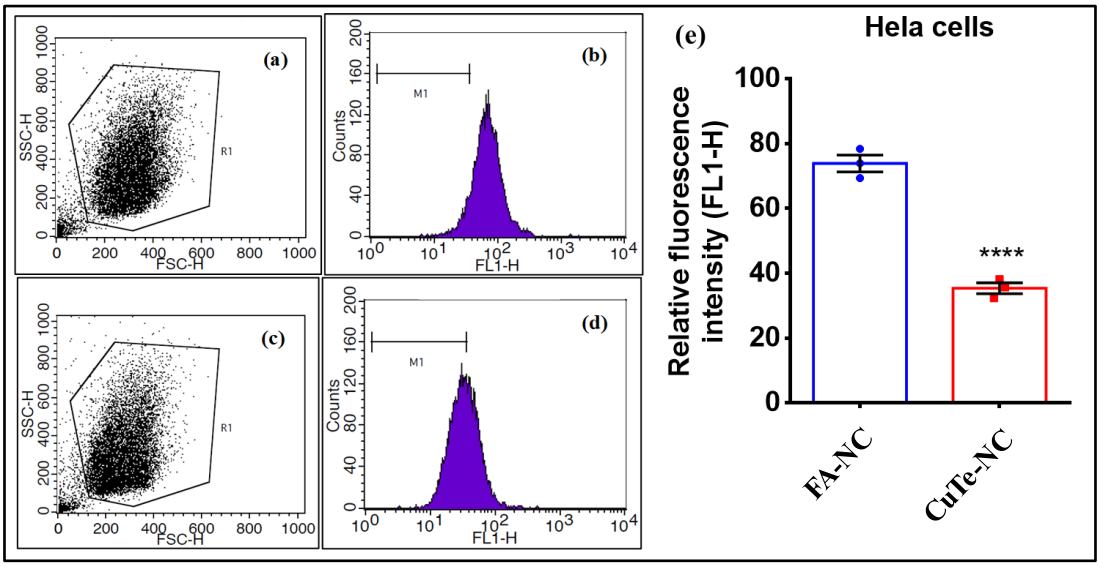

Figure 11: Flow cytometric analysis showing uptake of FA-NC/CuTe-NC nanocomposites in HeLa cells (a) Forward and side scatter (FSC–SSC) plots representing the gated cell populations of HeLa, (b) FL1-H fluorescence histograms depicting cellular internalization of

FA-NC nanocomposites; in HeLa Cells, (c) Forward and side scatter (FSC–SSC) plots representing the gated cell populations of HeLa. (d) FL1-H fluorescence histograms depicting cellular internalization of CuTe-NC nanocomposites in Hela cells. (e) The bar diagram displayed the fluorescence intensity for various treatment conditions.

The flow cytometric analysis also revealed a marked difference in the fluorescence intensity profiles of HeLa (Figure 12a and 12b) and CHO (Figure 12c and 12d) cells following incubation with FA-NC nanocomposites. The HeLa cells, which overexpress folate receptors on their surface, exhibited a distinct rightward shift in the FL1-H fluorescence histogram (mean intensity 75.76±5.3), which is approximately two-fold higher than that of CHO cells (mean intensity 37.4±2.2). This shift indicates enhanced internalization or surface binding of the FA-NC nanocomposites in HeLa. The CHO cells treated with the FA-NC showed similar fluorescence intensity when it was treated with CuTe-NC (Figure 12e and 12f). As FA receptors are very less in CHO cells, the internalization of FA tagged compound and untagged compound is almost similar. This result indicates that the both FA receptor and FA conjugation are required for effective fluorescence imaging.

In contrast, CHO cells displayed a broader but low-intensity fluorescence distribution (peak channel = 33), corresponding to nonspecific surface adsorption rather than active endocytosis. The shift of the fluorescence peak to channel 77 in HeLa cells confirms strong receptor–ligand interactions between folic acid and overexpressed folate receptors. Overall, the data establish that folate conjugation makes FA-NC nanocomposites into receptor-specific nanocarriers, capable of discriminating between cancerous and normal cells, which is critical for designing targeted diagnostic and therapeutic nanoplatforms. Figure 12g shows comparison in fluorescence intensity for various treatment conditions. However, since there was no observable fluorescence in HaCaT cells after treatment with FA-NC nanocomposites (figure 9d), flow cytometric analysis was not performed with HaCaT cells.

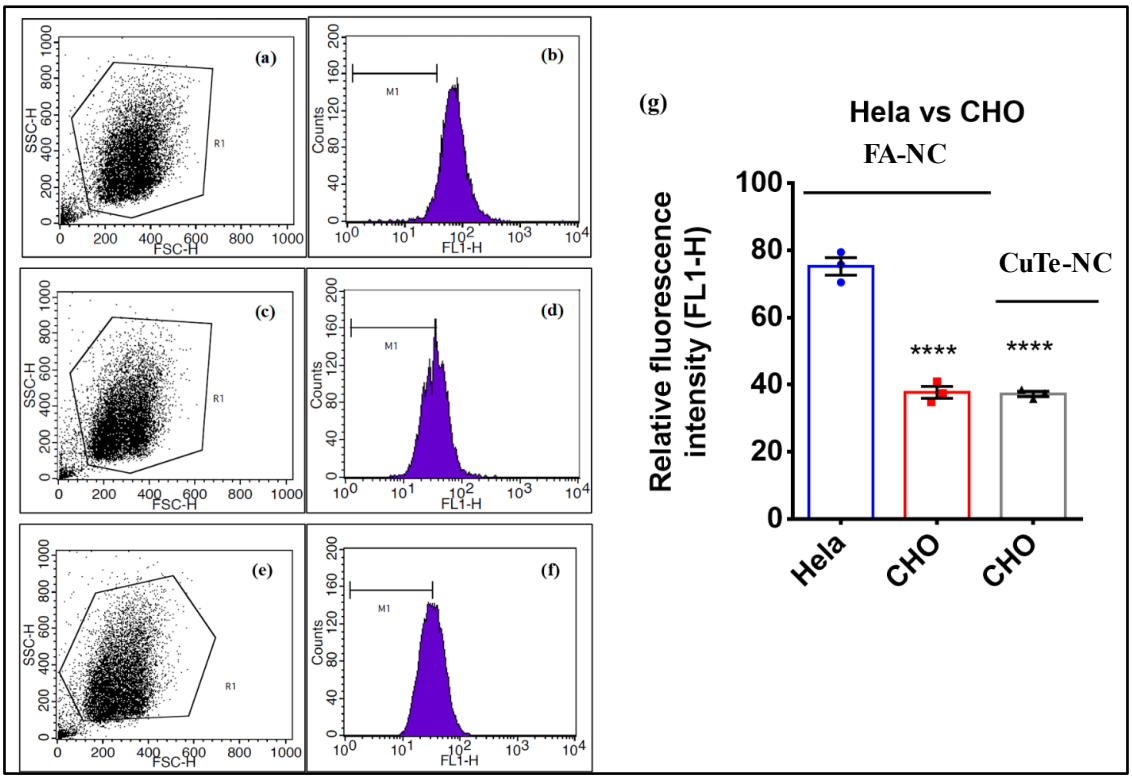

Figure 12: Flow cytometric analysis showing folate receptor–mediated uptake of folic acid–conjugated FA-NC nanocomposites in HeLa:(a) Forward and side scatter (FSC–SSC) plots representing the gated cell populations of HeLa, (b) FL1-H fluorescence histograms depicting cellular internalization of FA-NC nanocomposites; in CHO: (c) Forward and side scatter (FSC–SSC) plots representing the gated cell populations of CHO. (d) FL1-H fluorescence histograms depicting cellular internalization of FA-NC nanocomposites. (e) Forward and side scatter (FSC–SSC) plots representing the gated cell populations of CHO. (f) FL1-H fluorescence histograms depicting cellular internalization of CuTe-NC. (g) The bar diagram displayed the fluorescence intensity for various treatment conditions.

3.5. Antiproliferative Property of FA-NC towards HeLa Cells

To further explore the novel application of FA-NC nanocomposite for therapeutic purpose, cell viability assay was performed using human cervical cancer cells, HeLa. The cells were incubated with different concentrations of FA-NC ranging between 0-50 µg/mL. The antiproliferative activity of FA-NC was determined by monitoring the changes in growth of FA-NC treated HeLa cells. Figure 13 shows that plot of % viability of the cells against concentrations of nano FA-NC. It was clearly evident that FA-NC nanocomposite was able to exhibit significant cytotoxic effect towards HeLa cells in a dose-dependent manner with a

IC_{50} value of 15 µg/mL. This result validates the therapeutic potential of FA-NC nanocomposite along with its diagnostic potency as described above, indicating theranostic property of FA-NC nanocomposite against HeLa cells. The cytotoxic concentration (IC_{50} in the range of tens of µg/mL) observed in our system is consistent with previous reports on CuO nanoparticles against HeLa cells, for which IC_{50} value of 10.7 µg/mL have been documented [34]. The dose-response profile of CuTe-NC shows a moderate antiproliferative activity toward HeLa cells, as reflected in the gradual decline in cell viability with increasing CuTe-NC concentration. At lower doses (0-10 µg/mL), the decrease in viability is relatively mild, indicating limited cytotoxicity and largely nonspecific interactions with the cells. However, beyond that range, the viability curve begins to drop more noticeably, demonstrating that higher concentrations of CuTe-NC can impair HeLa cell proliferation to a certain extent. Despite this downward trend, the overall cytotoxic effect of CuTe-NC remains significantly weaker than that of FA-NC, as the CuTe-NC-treated cells retain comparatively higher viability at all concentrations. This behaviour is consistent with lack of folate in CuTe-NC. Therefore, the graph clearly indicates that while CuTe-NC exhibits inherent cytotoxicity at elevated doses, its therapeutic potency remains limited unless folic acid conjugation is introduced.

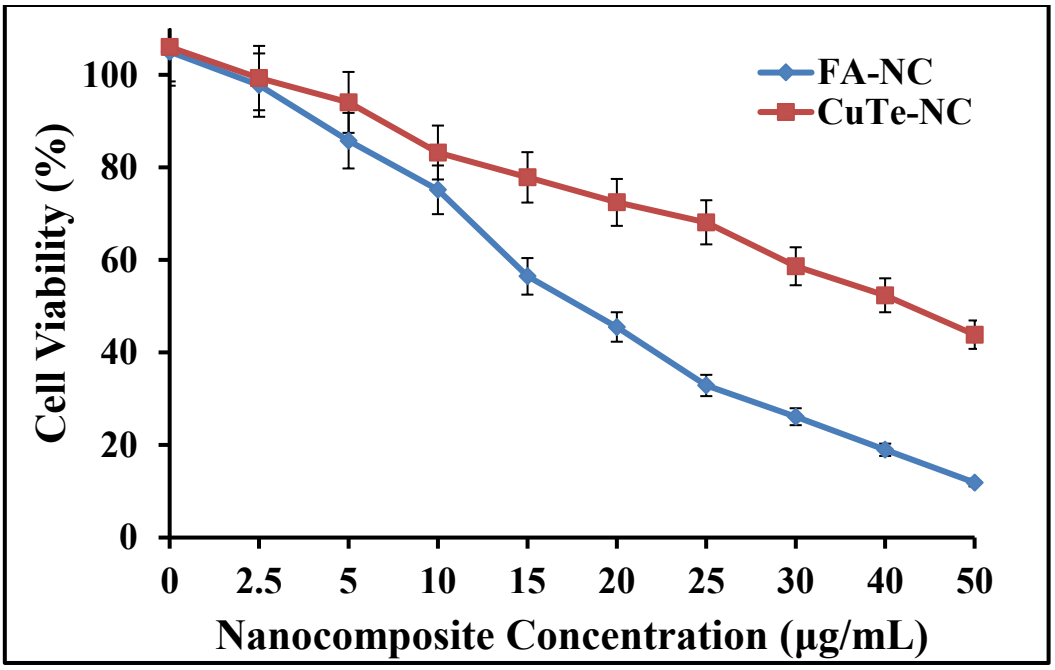

Figure 13: Variation of cell viability (%) of HeLa in presence of different concentrations of CuTe-NC and FA-NC nanocomposites (0-50 µg/mL).

3.6. Intracellular ROS Generation Assessment

Flow cytometric analysis was used to compare the extent of ROS generation in HeLa cells following treatment with CuTe-NC and FA-NC nanocomposites. Figure 14a shows the FSC–SSC gating strategy used to separate intact cells from debris prior to analysis. After 2h of treatment, the cancer cells (HeLa) treated with CuTe-NC showed a substantial increase in ROS generation in contrast to the control (Figure 14b). Notably, FA-NC induced a much more pronounced shift in DCF fluorescence, corresponding to a ~1.6-fold increase in ROS levels compared to CuTe-NC. This enhancement strongly suggests that folic-acid functionalization significantly improves intracellular delivery of FA-NC into folate receptor–positive HeLa cells, thereby amplifying oxidative stress. The bar diagram (Figure 14c) clearly highlights this trend, with FA-NC showing the highest DCF mean fluorescence intensity among all groups. The elevated ROS levels are consistent with the enhanced cytotoxicity observed in cell viability assays and indicate that FA-mediated uptake enables FA-NC to induce stronger oxidative damage, contributing to its therapeutic efficacy against HeLa cells. Together, these results confirm that FA-NC triggers superior ROS-mediated cytotoxicity, likely due to enhanced cellular internalization through folate receptor–mediated uptake.

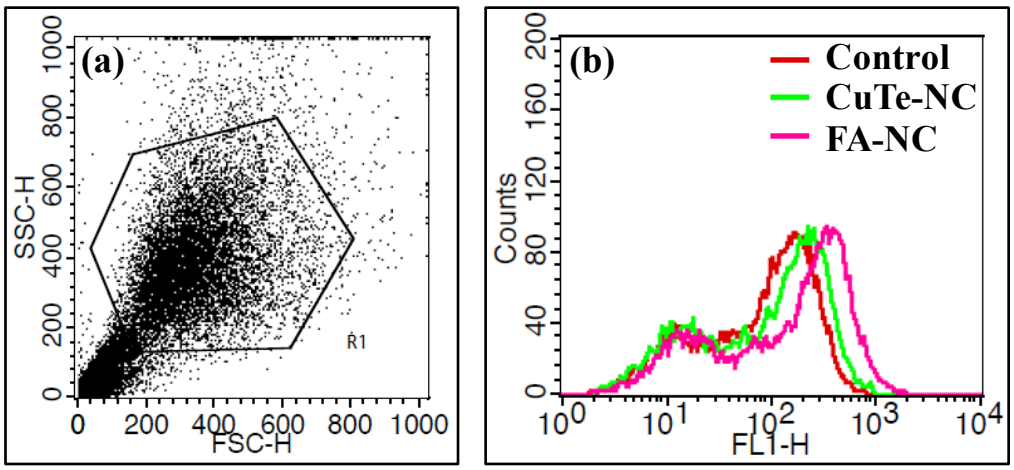

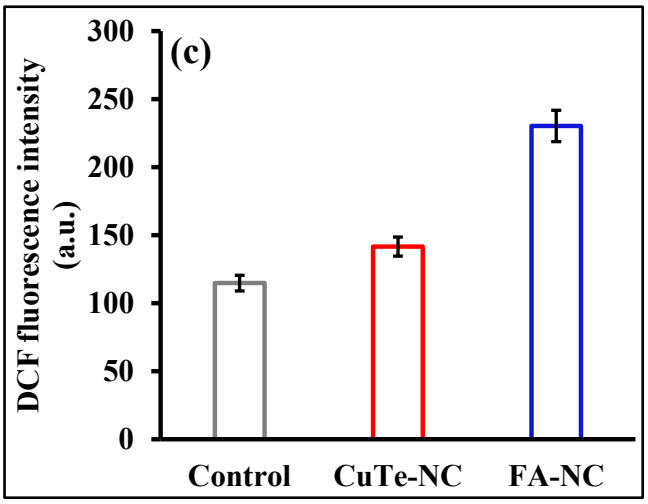

Figure 14: Evaluation of oxidative stress in HeLa cells. (A) A graph showing the separation of cell debris from total cell populations using the SSC-H vs. FSC-H plot. (B) An overlaid DCF fluorescence histograms showing ROS formation in control, CuTe-NC and FA-NC nanocomposites. The DCF intensity and count were measured using the X axis, the Y axis, and the FL1-H (green) channel, respectively. Different histogram colours corresponded to the ROS generation in different systems. (C) The bar diagram displayed the DCF mean fluorescence intensity for various systems.

3.7. Mitochondrial Membrane Potential Analysis

Flow cytometric analysis using JC-1 staining revealed clear differences in mitochondrial membrane potential among untreated, CuTe-NC treated, and FA-NC treated HeLa cells (Figure 15). Mitochondrial membrane potential was evaluated as excess ROS causes mitochondrial stress which in turn alters its membrane potential. Untreated HeLa cells (control) showed strongly polarized mitochondria, with 98.17% of cells in the JC-1 aggregate-rich red (UR) quadrant and only 1.83% in the green monomer (LR) quadrant (Figure 15a). This establishes a baseline of intact mitochondrial function under physiological conditions. Exposure to CuTe-NC induced a moderate loss of $\Delta\Psi m$, increasing the depolarized population to 8.80% (LR), which is a ~4.8-fold rise compared to the control (Figure 15b). The polarized fraction decreased from 98.17% to 91.19%, indicating partial mitochondrial injury. This moderate depolarization correlates with ability of CuTe-NC to generate ROS, although to a lesser extent due to nonspecific cellular uptake. FA-NC treatment caused a substantial collapse of the mitochondrial membrane potential, with significant increase of depolarized cell population in the LR quadrant (26.72%), 14.6-fold

higher than the control and ~3-fold higher than CuTe-NC (Figure 15c). The healthy polarized population dropped sharply to 73.27%, reflecting severe mitochondrial depolarization. This dramatic loss of ΔΨm by FA-NC is consistent with efficient folate receptor–mediated cellular uptake and thereby significantly higher ROS generation. Together, these results clearly demonstrate that FA-NC induces marked mitochondrial dysfunction, consistent with activation of the intrinsic (mitochondrial) apoptotic pathway.

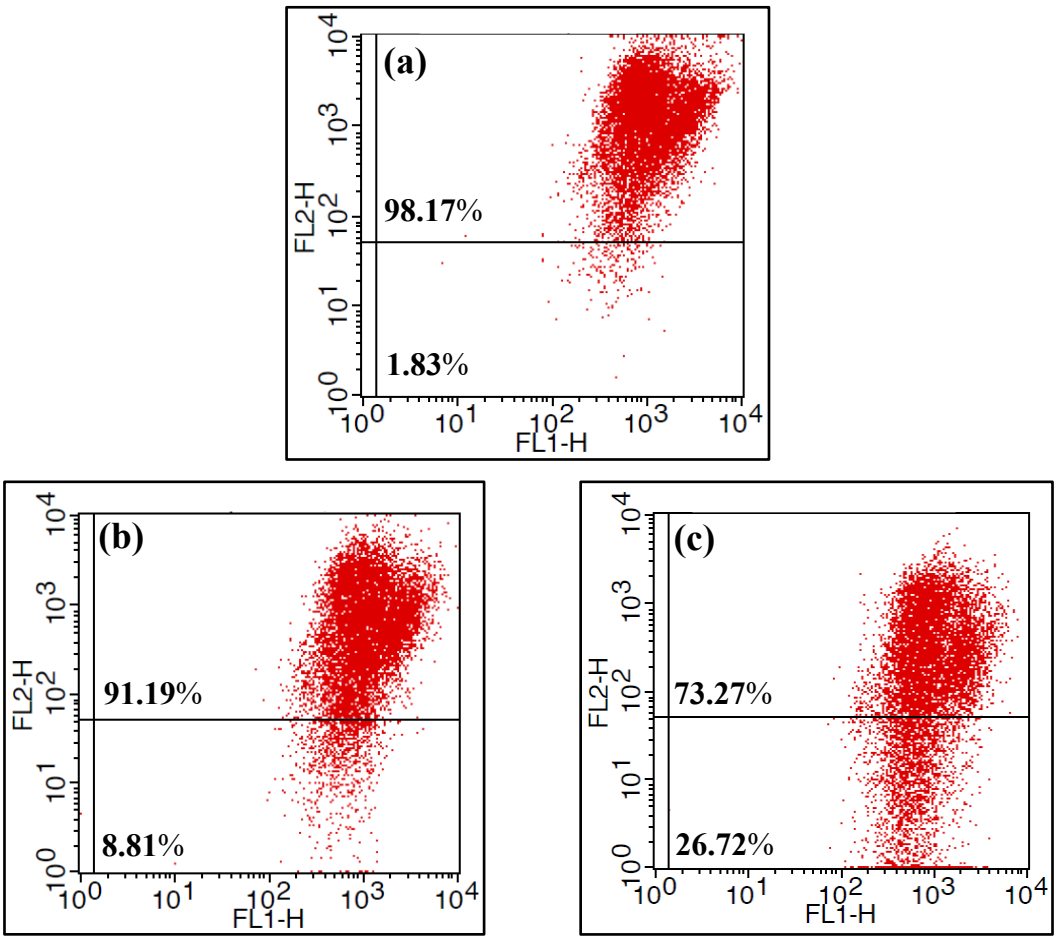

Figure 15: Flow cytometric evaluation of alteration in mitochondrial membrane potential: Dot plots demonstrate alteration of mitochondrial membrane potential in (a) untreated, (b) CuTe-NC treated, and (c) FA-NC treated HeLa cells. The top quadrant represents the cell population with no loss of mitochondrial membrane potential and the lower quadrant represents the cell population with loss of mitochondrial membrane potential (apoptotic population).

3.8. Plausible Reasons behind Therapeutic Activity of FA-NC Nanocomposite

Our fluorescence microscopic data reveals that the conjugation of folic acid on the surface of the CuTe-NC nanocomposite is responsible for the specificity of FA-NC nanocomposite towards folate receptor positive HeLa cells. Now to understand the reason behind the therapeutic potency of FA-NC nanocomposite, the interaction between FA-NC nanocomposite with BDNA was further investigated using experimental and theoretical techniques, which are described below. The observed groove-binding interaction between FA-NC and DNA aligns with earlier findings for small molecules and nanocomposite systems exhibiting hydrophobic groove association with B-DNA [35].

3.8.1. Isothermal Calorimetric Studies for DNA-FA-NC Interactions

The thermodynamic and binding parameters obtained from isothermal calorimetric study are as shown in Table 7. The measurements indicate 3 binding sites, that is, one DNA molecule being bound to three FA-NC nanocomposites. A negative value of change in Gibbs free energy indicates spontaneity of the interaction with a positive change in entropy being the driving force. Positive enthalpy change suggests an endothermic pathway of interaction (Figure 16). Both positive changes in enthalpy and entropy indicate hydrophobic association between FA-NC and DNA [36]. The dissociation constant value (K_d = 69.2 μM) indicates a moderate binding affinity between FA-NC and DNA.

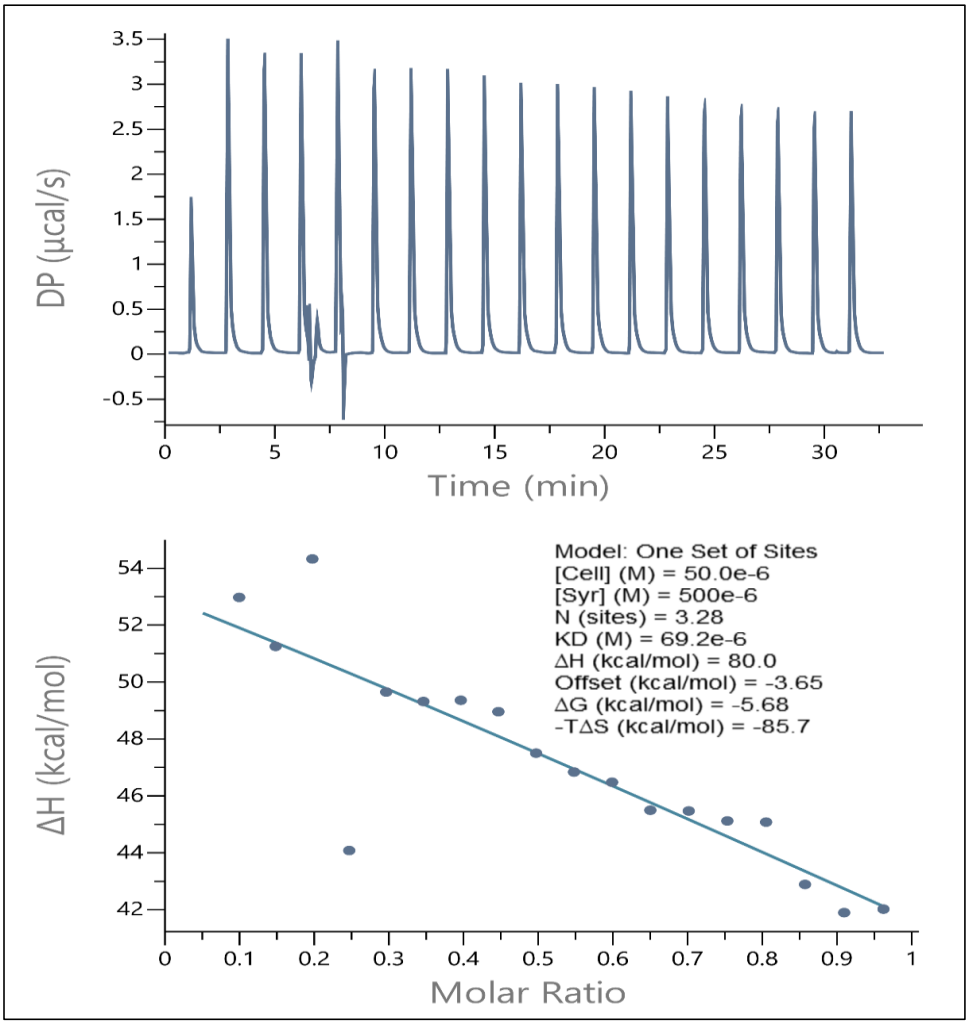

Figure 16: Isothermal calorimetric data for the binding of FA-NC with BDNA.

Table 7: Thermodynamic parameters associated with the binding of DNA with FA-NC

N (sites)	3.28±1.93
K_d (M)	$69.2\times10^{-6} \pm 3.31\times10^{-6}$
ΔH (kcal/mol)	80.0 ± 3.53
ΔG (kcal/mol)	-5.68
-TΔS (kcal/mol)	-85.7

3.8.2. CD Spectroscopic Study

Circular dichroism spectroscopy (Figure 17) exhibits two positive peaks at 218 and 275 nm and a negative peak at 245 nm, which agrees with the characteristic CD spectra of DNA

reported in literature [37]. The moderate changes in the secondary structure of DNA at both peaks of 218 and 275 nm were found in presence of increasing concentrations of FA-NC nanocomposite, which indicates a groove binding pattern of FA-NC towards DNA [38] along with slight structural alterations. Since the stacking connections of the base pairs of DNA make room for the intercalated FA-NC, the intercalation of this nanocomposite has a moderate impact on the CD spectrum of DNA. However, groove binders have less of an effect on the CD signal since they only modify the secondary structure of DNA. The gradual addition of FA-NC in the current study did not significantly alter the CD spectrum of DNA, indicating the presence of the groove binding interaction.

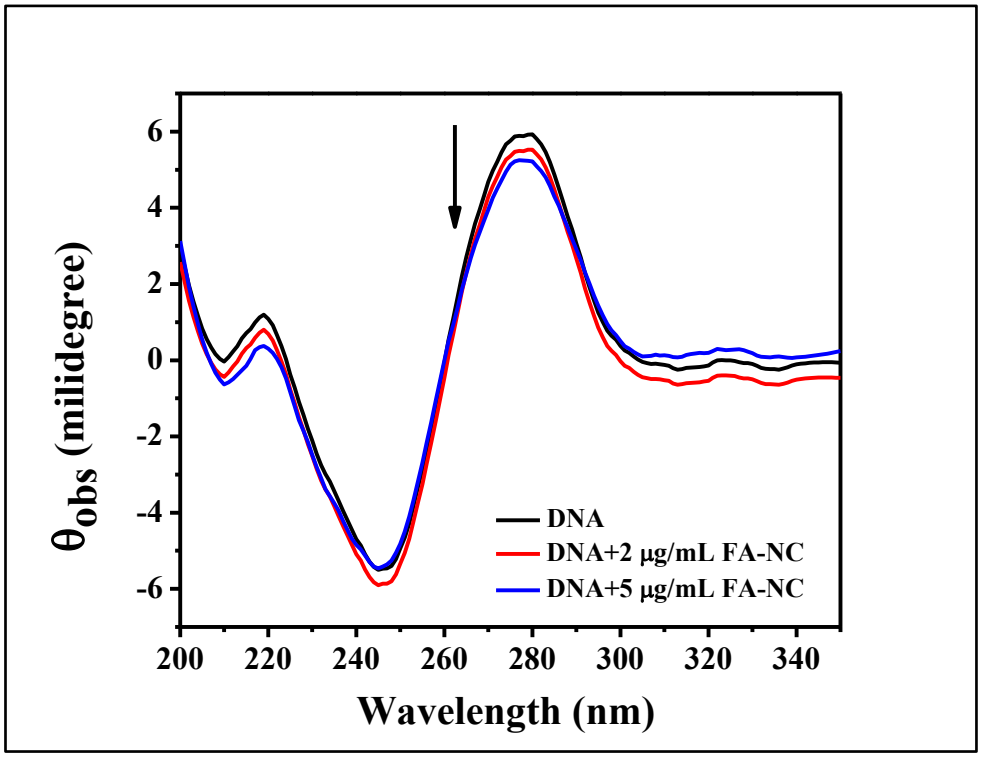

Figure 17: The changes in secondary structure of BDNA in presence of FA-NC nanocomposite.

3.8.3. Theoretical Study

The theoretical model for B-DNA was obtained from Protein Data Bank (PDB). The coordinates of FA-NC nanocomposite were designed using Avogadro software (Figure 18a). The structure of DNA-FA-NC was obtained by docking FA-NC nanocomposite with DNA (Figure 18b) and the total binding energy of the docked complex was found to be -677 kcal/mol. Our theoretical result also shows groove binding pattern of FA-NC nanocomposite,

which agrees with our CD studies as discussed above. List of different DNA base pairs interacting with FA-NC nanocomposite are shown in table 8. The docked structure indicates O atoms of the nano FA-NC take major part in interactions with A-T and G-C base pairs of DNA via noncovalent interaction (both hydrogen bonding and van der Waals interaction) (Figure 18c). However, some weak van der Waals interaction also occurs through Cu and Te metal counterpart of FA-NC with the DNA. Through reversible noncovalent interactions, FA-NC nanocomposite attaches to the edges of the base pairs of the DNA duplex, typically G-C sites in the major groove and A-T sites in the minor groove [39]. However, FA-NC nanocomposite primarily interacts with A-T base pair of DNA, which suggest minor groove binding. Typically, groove binding has little effect on significant structural or conformational alterations on the DNA duplex which is also suggested from CD spectroscopic results.

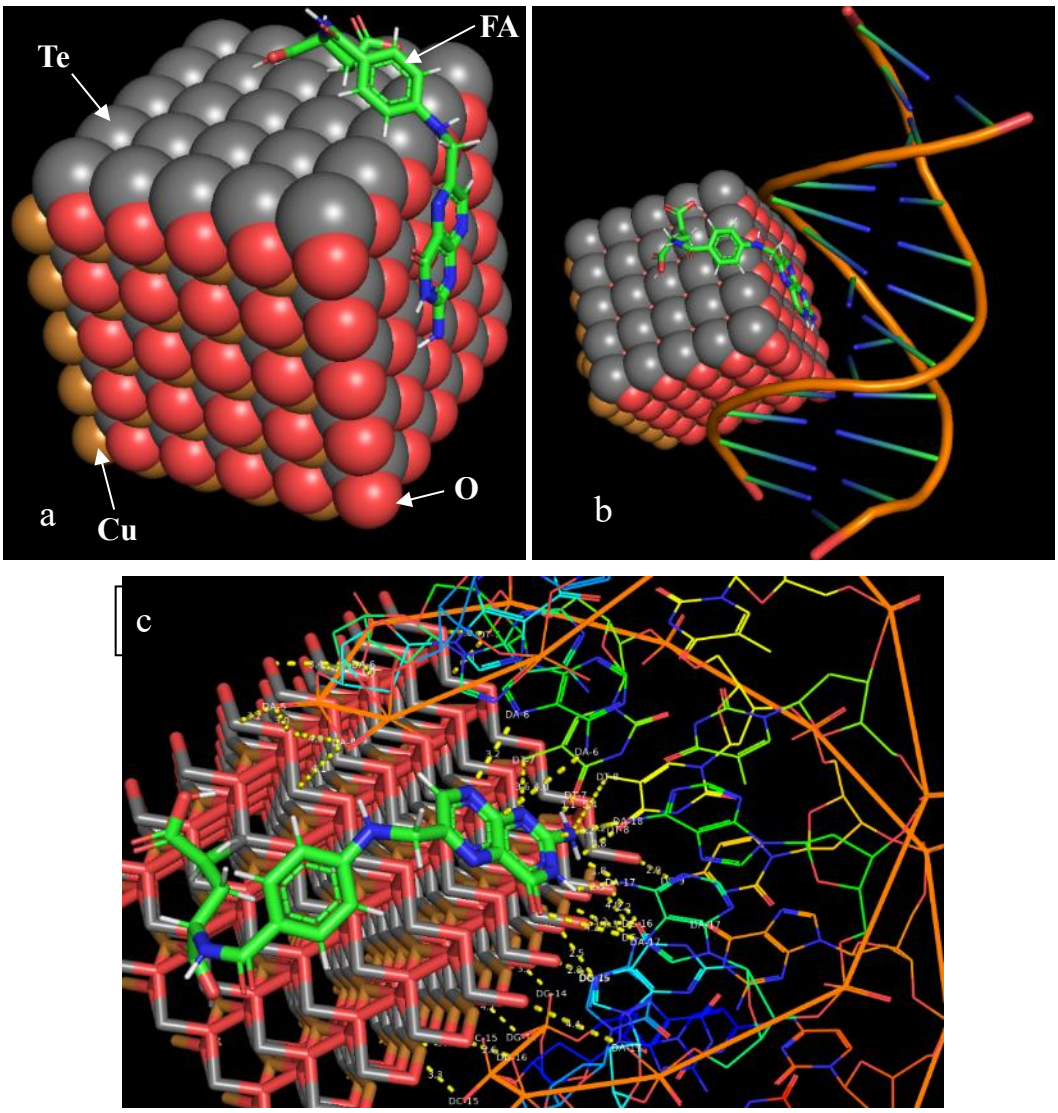

Figure 18: (a) Theoretical model of FA-NC nanocomposite; (b) Docked model for FA-NC-DNA; (C) Adjacent interacting with DNA bases towards FA-NC nanocomposite.

Table 8: List of DNA bases interacting with FA-NC nanocomposite

Binding domain of FA-NC	**Atom**	**DNA base***	**Bond length (Å)**
CuTe-NC	O	DA-5	3.0, 4.0
		DA-6	1.9, 3.4
		DC-15	2.5
		DG-16	2.2, 2.3, 2.6
		DT-7	3.0
		DA-17	4.4
		DC-9	2.9
	Cu	DC-15	3.2, 3.3, 4.5
		DG-14	3.2, 4.1
	Te	DA-5	3.2, 4.1
		DA-6	2.3
		DT-7	3.3
FA	N	DT-7	3.6
	N	DA-6	3.2
	N	DT-8	3.4
	C, N	DA-18	3.2
	C	DA-6	4.0
	H	DT-8	2.8
	H	DT-7	1.1
	H	DA-17	1.8, 2.5
	O	DA-17	4.2

*DA, adenine; DG, guanine; DT, thymine; DC, cytosine

4. Conclusion

The unique optical properties of nanocomposites offer a plethora of advantages in terms of their usage in bioimaging and biosensing. The intrinsic fluorescence properties of the FA-NC

nanocomposite have led to its applicability in both diagnostic and therapeutic fronts. In this study, FA-NC nanocomposite has proven specific binding to folate receptor overexpressed cancer cells which makes it efficient in imaging as well as their quantitative detection. FA-NC nanocomposite is also found to function as fluorosensor for sensitive detection of HeLa cells with LOD value of 1.82×10^3 cells/mL. Moreover, FA-NC nanocomposite exerted antiproliferative property against HeLa with IC50 of 15 μg/mL, offering a good choice to be used as theranostic agent against HeLa cells. The DNA binding ability of FA-NC nanocomposite may justify its antiproliferative property which has also shown satisfactory results as a biosensor for DNA. Apart from its selectivity and high sensitivity, the green approach for the synthesis of FA-NC nanocomposite also makes it a cost effective theranostic agent for future applications. While the FA-NC nanocomposite demonstrates promising theranostic potential, further investigations are required to evaluate its long-term stability*, in-vivo* biocompatibility, pharmacokinetics, and biodistribution. Future research should focus on detailed mechanistic analyses of cellular uptake and DNA interactions. Long-term toxicity, particularly in normal tissues, can also be explored. Optimization of dosage could enhance its applicability in clinical imaging and therapy.

Acknowledgments

DD acknowledges the award and funding of CSIR SRA fellowship (B-12827). We thank DST FIST (SR/FST/CS-II/2017/27(C) dated 29.09.2018) for funding the ITC instrument. We appreciate the help in getting DLS, FTIR and fluorescence data from Dr. Goutam Pramanik and Dr. Aparna Datta of the UGC-DAE Consortium for Scientific Research in Kolkata, India. We thank the University of Calcutta's Department of Physics for funding the DST-PURSE (Phase II) initiative, which allowed for the purchase and installation of a Raman spectrometer.

References:

1. F. Castro-Giner, N. Aceto, Tracking cancer progression: from circulating tumor cells to metastasis, Genome. Med. 12 (1) (2020) 31. https://doi.org/10.1186/s13073-020-00728-3
2. J. I. Omage, E. Easterday, J. T. Rumph, I. Brula, B. Hill, J. Kristensen, D. T. Ha, C. L. Galindo, M. K. Danquah, N. Sims, V. T. Nguyen, Cancer Diagnostics and Early Detection Using Electrochemical Aptasensors, Micromachines. 13 (4) (2022) 522. https://doi.org/10.3390/mi13040522

3. S. Hussain, I. Mubeen, N. Ullah, S. S. U. D. Shah, B. A. Khan, M. Zahoor, R. Ullah, F. A. Khan, M. A. Sultan, Modern Diagnostic Imaging Technique Applications and Risk Factors in the Medical Field: A Review, Biomed. Res. Int. 2022 (1) (2022) 5164970. DOI: https://doi.org/10.1155/2022/5164970
4. D. Lother, M. Robert, E. Elwood, S. Smith, N. Tunariu, S. R. D. Johnston, M. Parton, B. Bhaludin, T. Millard, K. Downey, B. Sharma, Imaging in metastatic breast cancer, CT, PET/CT, MRI, WB-DWI, CCA: review and new perspectives, Cancer. Imaging. 23 (1) (2023) 53. https://doi.org/10.1186/s40644-023-00557-8
5. A. Refaat, M. L. Yap, G. Pietersz, A. P. G. Walsh, J. Zeller, B. del Rosal, X. Wang, K. Peter, In vivo fluorescence imaging: success in preclinical imaging paves the way for clinical applications, J. Nanobiotechnol. 20 (1) (2022) 450. https://doi.org/10.1186/s12951-022-01648-7
6. N. I. Georgiev, V. V. Bakov, K. K. Anichina, V. B. Bojinov, Fluorescent Probes as a Tool in Diagnostic and Drug Delivery Systems, Pharmaceuticals. 16 (3) (2023) 381. https://doi.org/10.3390/ph16030381
7. H. Lan, M. Jamil, G. Ke, N. Dong, The role of nanoparticles and nanomaterials in cancer diagnosis and treatment: a comprehensive review, Am. J. Cancer Res. 13 (12) (2023) 5751–5784. https://pubmed.ncbi.nlm.nih.gov/38187049/
8. F. Ahmad, M. M. Salem-Bekhit, F. Khan, S. Alshehri, A. Khan, M. M. Ghoneim, H. F. Wu, E. I. Taha, I. Elbagory, Unique properties of surface-functionalized nanoparticles for bio-application: functionalization mechanisms and importance in application, Nanomaterials. 12 (8) (2022) 1333. https://doi.org/10.3390/nano12081333
9. E. C. Dreaden, A. M. Alkilany, X. Huang, C. J. Murphy, M. El-Sayed, The golden age: gold nanoparticles for biomedicine, Chem. Soc. Rev. 41 (7) (2011) 2740–2779. https://doi.org/10.1039/c1cs15237h
10. V. Biju, T. Itoh, A. Anas, A. Sujith, M. Ishikawa, Semiconductor quantum dots and metal nanoparticles: syntheses; optical properties; and biological applications, Anal. Bioanal. Chem. 391 (7) (2008) 2469–2495. https://doi.org/10.1007/s00216-008-2185-7
11. Y. Song, W. Shi, W. Chen, X. Li, H. Ma, Fluorescent carbon nanodots conjugated with folic acid for distinguishing folate-receptor-positive cancer cells from normal cells, J. Mater. Chem. 22 (25) (2012) 12568-12573. https://doi.org/10.1039/C2JM31582C
12. Y. Wen, J. Wang, W. Zheng, J. Zhu, X. Song, T. Chen, M. Zhang, Z. Huang, J. Li, A supramolecular colloidal system based on folate-conjugated β-cyclodextrin polymer and indocyanine green for enhanced tumor-targeted cell imaging in 2D culture and 3D tumor

spheroids, J. Colloid. Interface. Sci. 667 (2024) 259-268. https://doi.org/10.1016/j.jcis.2024.04.072

13. D. J. Bharali, D. W. Lucey, H. Jayakumar, H. E. Pudavar, P. N. Prasad, Folate-receptor-mediated delivery of InP quantum dots for bioimaging using confocal and two-photon microscopy, J. Am. Chem. Soc. 127 (32) (2005) 11364-11371. https://doi.org/10.1021/ja051455x
14. M. Geszke, M. Murias, L. Balan, G. Medjahdi, J. Korczynski, M. Moritz, J. Lulel, R. Schneider, Folic acid-conjugated core/shell ZnS: Mn/ZnS quantum dots as targeted probes for two photon fluorescence imaging of cancer cells, Acta. Biomater. 7 (3) (2011) 1327-1338. https://doi.org/10.1016/j.actbio.2010.10.012
15. A. J. Marko, B. M. Borah, K. E., Siters, J. R. Missert, A. Gupta, P. Pera, M. F. Isaac-Lam, Pandey, R. K, Targeted nanoparticles for fluorescence imaging of folate receptor positive tumors, Biomolecules. 10 (12) (2020) 1651. https://doi.org/10.3390/biom10121651
16. A. Saffar, T. R. Bastami, A. Ebrahimi, S. Iranpour, M. H. Mollaei, A. R. Bahrami, M. M. Matin, Enhancing Anticancer Effects: Targeted Doxorubicin Delivery Using UiO-66-NH2-FA Metal-Organic Framework Combined with Autophagy Inhibition by Hydroxychloroquine in Colorectal Cancer Cells, J. Mater. Sci.: Mater. Med. 36 (1) (2025) 1-16. https://doi.org/10.1007/s10856-025-06913-3
17. N. Jamshidi, A. Tarighatnia, M. F. Ghaziyani, F. Sajadian, M. Olad-Ghaffari, N. D Nader, Folic acid-conjugated Fe-Au-based nanoparticles for dual detection of breast cancer cells by magnetic resonance imaging and computed tomography, Frontiers. Biomed. Technol. 11 (1) (2023). https://doi.org/10.18502/fbt.v11i1.14519
18. P. Pandit, S. Bhagat, P. Rananaware, Z. Mohanta, M. Kumar, V. Tiwari, S. Singh, , V. P. Brahmkhatri, Iron oxide nanoparticle encapsulated; folic acid tethered dual metal organic framework-based nanocomposite for MRI and selective targeting of folate receptor expressing breast cancer cells, Micropor. Mesopor. Mat. 340 (2022) 112008. https://doi.org/10.1016/j.micromeso.2022.112008
19. Z. Zhou, C. Zhang, Q. Qian, J. Ma, P. Huang, X. Zhang, L. Pan, G. Gao, H. Fu, S. Fu, H. Song, X. Zhi, J. Ni, D. Cui, Folic acid-conjugated silica capped gold nanoclusters for targeted fluorescence/X-ray computed tomography imaging. J. Nanobiotechnol. 11 (1) (2013) 17. https://doi.org/10.1186/1477-3155-11-17

20. A. T. R. Williams, S. A. Winfield, J. N. Miller, Relative fluorescence quantum yields using a computer-controlled luminescence spectrometer. Analyst. 108 (1290) (1983) 1067-1071. https://doi.org/10.1039/AN9830801067
21. D. Das, S. Basu, S. Ray, S. Koppayithodi, B. Hazra, S. Bandyopadhyay, A. Saha, K. Sen, Generation of selenium nanoparticles under γ-Irradiation for optical sensing of carcinoembryonic antigen, J. Mol. Liq. 361 (2022) 119597. https://doi.org/10.1016/j.molliq.2022.119597
22. T. Banerjee, U. Das, A. Bose, K. Sen, Chitosan anchored lecithin-cholesterol liposomes for cisplatin encapsulation and favourable sustained release to HeLa cells. BioNanoSci. 15 (1) (2025) 80. https://doi.org/10.1007/s12668-024-01608-5
23. U. Das, A. Sengupta, S. Biswas, A. Adhikary, R. Dey Sharma, A. Chakraborty, S. Dey, Alteration of murine duodenal morphology and redox signalling events by reactive oxygen species generated after whole body γ-irradiation and its prevention by ferulic acid. Free Radic. Res. 51 (11-12) (2017) 886-910. https://doi.org/10.1080/10715762.2017.1388916
24. D. Das, M. Patra, A. Chakrabarti, Binding of hemin, hematoporphyrin, and protoporphyrin with erythroid spectrin: fluorescence and molecular docking studies, Eur. Biophys. J. 44 (2015) 171–182. https://doi.org/10.1007/s00249-015-1012-2
25. G. Macindoe, L. Mavridis, V. Venkatraman, M. D. Devignes, D. W. Ritchie, Hex Server: an FFT-based protein docking server powered by graphics processors, Nucleic. Acids. Res. 38 (2010) W445–W449. https://doi.org/10.1093/nar/gkq311
26. H. K. Ardani, C. Imawan, W. Handayani, D. Djuhana, A. Harmoko, V Fauzia, Enhancement of the stability of silver nanoparticles synthesized using aqueous extract of Diospyros discolor Willd. leaves using polyvinyl alcohol, In IOP Conference Series: Materials Science and Engineering (Vol. 188, No. 1, p. 012056) (2017) IOP Publishing.
27. M. O. Reese, C. L. Perkins, J. M. Burst, S. Farrell, T. M. Barnes, S. W. Johnston, D. Kuciauskas, T. A. Gessert, W. K. Metzger, Intrinsic surface passivation of CdTe, J. Appl. Phys. 118 (2015) 155305. https://doi.org/10.1063/1.4933186
28. K. A. Rawat, R. K Singhal, S. K. Kailasa, One-pot synthesis of silver nanoparticles using folic acid as a reagent for colorimetric and fluorimetric detections of 6-mercaptopurine at nanomolar concentration, Sens. Actuator B-Chem. 249 (2017) 30-38. https://doi.org/10.1016/j.snb.2017.04.018
29. A. Trivedi, J. Thakarda, N. Chavda, Y. K. Agrawal, P. Maity, A new route towards selective synthesis of supported Cu_2O and CuO nanoparticles under extremely mild

condition, Nano-Struct. Nano-Objects. 6 (2016) 34–38. http://dx.doi.org/10.1016/j.nanoso.2016.03.004

30. S. N. Yannopoulos, Structure and photo-induced effects in elemental chalcogens: a review on Raman scattering, J. Mater. Sci. Mater. Electron. 31 (2020) 7565–7595. https://doi.org/10.1007/s10854-020-03310-0
31. M. Ahmadi, C. A. Ritter, T. von Woedtke, S. Bekeschus, K Wende, Package delivered: folate receptor-mediated transporters in cancer therapy and diagnosis. Chem. Sci. 15 (6) (2024) 1966-2006. https://doi.org/10.1039/d3sc05539f
32. J. M. Xia, X. Wei, X. W. Chen, Y. Shu, J. H. Wang, Folic acid modified copper nanoclusters for fluorescent imaging of cancer cells with over-expressed folate receptor. Microchim. Acta. 185 (3) (2018) 205. https://doi.org/10.1007/s00604-018-2743-4
33. T. E. Kim, H. J. Jang, S. W. Park, J. Wei, S. Cho, W. I. Park, B. R. Lee, C. D. Yang, Y. K. Jung, Folic acid functionalized carbon dot/polypyrrole nanoparticles for specific bioimaging and photothermal therapy. ACS Appl. Bio Mater. 4 (4) (2021) 3453-3461. https://doi.org/10.1021/acsabm.1c00018
34. F. A. Ras, G. Özhan, M. Abudayyak, Cyto-and genotoxicity of copper (II) oxide (CuO) nanoparticles in HeLa cells. İstanbul J. Pharm. 53 (2) (2023) 126-132. https://doi.org/10.26650/IstanbulJPharm.2023.1255310
35. M. Shakir, M. S. Khan, S. I. Al-Resayes, U. Baig, P. Alam, R. H. Khan, M. Alam, In vitro DNA binding, molecular docking and antimicrobial studies on a newly synthesized poly (o-toluidine)–titanium dioxide nanocomposite. RSC Adv. 4 (74) (2014) 39174-39183. https://doi.org/10.1039/C4RA05173D
36. P. D. Ross, S. Subramanian, Thermodynamics of protein association reactions: forces contributing to stability, Biochemistry. 20 (1981) 3096–3102. https://doi.org/10.1021/bi00514a017
37. S. Roy, Binding affinity of pyrano[3,2-f]quinoline and DNA: spectroscopic and docking approach, J. Biomol. Struct. Dyn. 36 (2018) 3869–3877. https://doi.org/10.1080/07391102.2017.1402710
38. G. S. Khan, A. Shah, Z. Rehman, D. Barker, Chemistry of DNA minor groove binding agents, J. Photochem. Photobiol. 115 (2012) 105–118. https://doi.org/10.1016/j.jphotobiol.2012.07.003
39. S. Bhaduri, N. Ranjan, D. P Arya, An overview of recent advances in duplex DNA recognition by small molecules. Beilstein J. Org. Chem. 14 (2018) 1051-1086. https://doi.org/10.3762/bjoc.14.93